Dopamine Neurons Mediate Learning and Forgetting through Bidirectional Modulation of a Memory Trace

Jacob A. Berry[1,*], **Anna Phan**[1], and **Ronald L. Davis**[1,2,*]

[1]Department of Neuroscience, The Scripps Research Institute Florida, Jupiter, FL 33458, USA

[2]Lead Contact

SUMMARY

It remains unclear how memory engrams are altered by experience, such as new learning, to cause forgetting. Here, we report that short-term aversive memory in *Drosophila* is encoded by and retrieved from the mushroom body output neuron MBOn-$\gamma 2\alpha'1$. Pairing an odor with aversive electric shock creates a robust depression in the calcium response of MBOn-$\gamma 2\alpha'1$ and increases avoidance to the paired odor. Electric shock after learning, which activates the cognate dopamine neuron DAn-$\gamma 2\alpha'1$, restores the response properties of MBOn-$\gamma 2\alpha'1$ and causes behavioral forgetting. Conditioning with a second odor restores the responses of MBOn-$\gamma 2\alpha'1$ to a previously learned odor while depressing responses to the newly learned odor, showing that learning and forgetting can occur simultaneously. Moreover, optogenetic activation of DAn-$\gamma 2\alpha'1$ is sufficient for the bidirectional modulation of MBOn-$\gamma 2\alpha'1$ response properties. Thus, a single DAn can drive both learning and forgetting by bidirectionally modulating a cellular memory trace.

In Brief

In *Drosophila*, dopamine neurons regulate both learning and forgetting. Berry et al. identify a locus for the storage and retrieval of a short-term memory trace and show that a single dopamine neuron regulates both formation and disruption of this trace. These findings elucidate circuit mechanisms underlying memory storage and removal.

Graphical Abstract

INTRODUCTION

Animals have evolved associative memory systems to rapidly and robustly adapt their behavior in response to environmental cues that accompany and thus potentially predict impactful outcomes. However, a lifetime in a complex world would inevitably produce a large number of erroneous associations or an ever-increasing load of correct associations that could saturate the memory system. For optimal cognitive flexibility, memory circuits must balance the formation of strong and enduring memories with the removal or updating of memories required by a changing environment (Richards and Frankland, 2017; Davis and Zhong, 2017). Disruptions in forgetting processes would lead to the loss of critical memories or the persistence of harmful ones, creating pathological conditions that could include dementia, drug addiction, and post-traumatic stress disorder. Thus, it is critical to understand the biological mechanisms for memory formation, memory updating, and memory removal.

Fruit flies form strong negative olfactory associations when an odor (conditioned stimulus, CS) is paired with a punishing electric shock (unconditioned stimulus, US), and these memories critically depend on the mushroom bodies (MBs) for their formation, storage, and retrieval (Davis, 1993; Heisenberg, 2003; Busto et al., 2010). Within the MB, odors activate sparse and unique sets of MB neurons (MBns) from an array of ~2000 in each hemisphere that in turn provide synaptic input to the dendrites of multiple MB output neurons (MBOns) via discrete axonal compartments along the length of the axon (Turner et al., 2008; Tanaka et al., 2008; Campbell et al., 2013; Aso et al., 2014a). The majority of the MBOn network appears divided into two mutually antagonistic classes that drive either approach or avoidance behavior (Aso et al., 2014b). Each MBn:MBOn compartment is innervated by specific cognate dopamine neurons (DAns) (Aso et al., 2014a), many of which respond to either rewarding or punishing stimuli and are necessary and sufficient, as a US, for memory formation (Mao and Davis, 2009; Schwaerzel et al., 2003; Claridge-Chang et al., 2009; Liu et al., 2012; Lin et al., 2014). Therefore, the MB is thought to store associative memory

engrams as sparse and DAn-mediated modifications in the connectivity of MBns to the MBOn network, and MBOns are the primary MB effectors of behavior during memory retrieval (Aso et al., 2014b). Consistent with this model, several MBOns have been implicated in the retrieval of aversive or appetitive memories, and the response properties of some MBOns are altered to odors paired with rewarding or punishing US, or artificial DAn activation (Séjourné et al., 2011; Plaçais et al., 2013; Owald et al., 2015; Bouzaiane et al., 2015; Hige et al., 2015; Cohn et al., 2015; Perisse et al., 2016; Yamazaki et al., 2018).

Changes in the response properties of an MBOn involved in memory retrieval that are created by aversive learning represent cellular memory traces that are likely components of the aversive memory engram (Davis and Zhong, 2017). The full aversive memory engram is undoubtedly spread across many MBOns, and the full list of MBOns involved in aversive memory is presently lacking. DAns belonging to the PPL1 cluster that are activated by punishing electric shock and are critical to aversive memory formation correspond to MBOns that drive approach, suggesting that these compartments are likely sites for aversive memory storage. While prior work has implicated some of these approach MBOns in aversive memory, curiously one, the MBOn-$\gamma2\alpha'1$, was recently shown to play a role in appetitive memory but not aversive memory (Yamazaki et al., 2018). Thus, despite the fact that its cognate DAn belongs to the PPL1 cluster and is strongly activated by electric shock, the role of MBOn-$\gamma2\alpha'1$ in aversive memory remains in question.

After aversive learning, the initially robust memory is forgotten rather rapidly across ~24 hr. We previously discovered that activity within a small set of PPL1 DAns, including DAn-$\gamma2\alpha'1$, is critical not only for the formation of aversive memory but also for the forgetting of these memories (Berry et al., 2012, 2015; Plaçais et al., 2012; Aso and Rubin, 2016). These findings suggest that these DAns, activated during learning, promote the formation of cellular memory traces in their corresponding MBn:MBOn compartments, with their subsequent activity disrupting these memory traces to cause forgetting. Other studies have shown that artificial DAn activation can alter odor-specific plasticity in some MBOns (Cohn et al., 2015; Hattori et al., 2017), presumably through the modulation of MBn:MBOn synapses. However, these studies did not synthesize the formation and disruption of cellular memory traces in MBOns with acquisition and forgetting of associative memory. Even in cases in which a cellular memory trace forms in parallel with learning, behavioral forgetting may function by disrupting the memory trace or by overriding an existing memory trace through changes in other parts of the circuit. In addition, it remains unknown what happens to a memory trace formed with one odor when a second odor is learned.

Here, we use *in vivo* functional imaging of MBOn physiology before and after learning and forgetting paradigms using aversive US stimuli, optogenetic control of DAns, and memory retrieval assays to determine whether a single DAn can both form and disrupt memory traces. We report that coincidence of odor and electric shock creates an immediate cellular memory trace in MBOn-$\gamma2\alpha'1$, and the retrieval of aversive memories immediately after learning require this MBOn. This memory trace manifests as a fully depressed MBOn-$\gamma2\alpha'1$ response specifically to the paired odor, likely due to changes in odor-specific MBn:MBOn-$\gamma2\alpha'1$ synapses. In addition, subsequent activation of DAn-$\gamma2\alpha'1$ using electric shock or optogenetics restores the normal odor-response properties of MBOn-

γ2α′1. This represents the disruption of the odor-specific memory trace. Parallel conditioning experiments indicate that this cellular memory trace and its disruption are relevant to learning and forgetting.

RESULTS

MBOn-γ2α′1 Receives Synaptic Input from MBn, and Its Output Is Required for Aversive Memory Retrieval

Previously, we demonstrated that the PPL1 DAns, including those in the γ2α′1 circuit (also known as MV1), play a dual role in both the learning and forgetting of aversive olfactory memory (Berry et al., 2012; 2015; Aso and Rubin, 2016). Therefore, we hypothesized that a part of the aversive memory engram is likely stored in the MBn:MBOn-γ2α′1 compartment (Figure 1A) as a cellular memory trace, and that subsequent activation of Dan-γ2α′1 may alter and disrupt this memory trace.

MBOn-γ2α′1 consists of two unipolar neurons in each hemisphere, with dendritic projections inside and presynaptic terminals outside the MB neuropil. The dendrites of these neurons innervate the MB neuropil at the junction between the vertical and horizontal lobes (Figures 1A–1C and S1A; Aso et al., 2014a). This architecture suggests that the MBOn-γ2α′1 dendrites likely integrate synaptic input across the dense array of MBn axons. Sitaraman et al. (2015) have shown functional connectivity between MBns and MBOn-γ2α′1. To test that the functional connectivity is due to a direct synaptic interaction, we used the synaptic GRASP (GFP reconstructed across synaptic partners, Macpherson et al., 2015) technique, coupled with confocal (Figure S1B) and structured illumination microscopy (SIM; Figures 1D and S1C). We found that the MBn axons do form presynaptic connections with MBOn-γ2α′1 that broadly cover the γ2 and α′1 compartments.

A recent study failed to find a role for MBOn-γ2α′1 in aversive memory when tested at 2 hr after learning (Yamazaki et al., 2018). To probe this neuron's role in short-term aversive memory, we blocked MBOn-γ2α′1 synaptic output via expression of temperature-sensitive shibire (shi^{ts1}; Kitamoto, 2001), either during acquisition and retrieval 1.5 min later (Figure 1E) or specifically during retrieval 5 min after acquisition (Figure 1F). We found that blocking MBOn-γ2α′1 output in either case caused a significant disruption of short-term memory performance. Because blocking only during retrieval was sufficient to disrupt short-term memory, these behavioral data strongly support the conclusion that short-term memory is encoded in and retrieved by MBOn-γ2α′1 and is a potential site of a short-term cellular memory trace.

Aversive Learning Creates a Robust Short-Term Memory Trace in MBOn-γ2α′1

To investigate the physiological responses of MBOn-γ2α′1 during learning and forgetting, we developed an *in vivo* functional imaging approach allowing simultaneous exposure of flies to odor and electric shock (the US) via the same shock grid used in standard behavioral assays (Figure 2A). We chose to use electric shock in our initial experiments because it represents a true aversive stimulus to the fly, rather than using artificial methods to activate DAns (Cohn et al., 2015; Hige et al., 2015). DAn-γ2α′1 responded to the standard 90 V,

123 shock protocol used in the field with robust Ca^{2+} transients in its synaptic terminals as detected by $GCaMP^{6f}$ expression (Figures 2B–2D), validating our setup and confirming prior studies (Mao and Davis, 2009; Cervantes-Sandoval et al., 2017). Next, we expressed $GCaMP^{6f}$ in MBOn-γ2α′1 (Figures 2E and 2F) and measured its response to MCH and OCT odors before (pre) and after (post) the standard associative learning paradigm, pairing an odor (CS^+) with 12 electric shock pulses (US) followed by an unpaired odor (CS^-) in the absence of shock pulses (paired group, P, Figure 2G). This associative conditioning schedule produces robust aversive memory, whereas an unpaired schedule (unpaired group, UP), which eliminates the contiguity between the CS^+ and US, produces no conditioned behavior. We found that MBOn-γ2α′1 (both dendrites and axon tracts) in naive flies responds robustly with a Ca^{2+} increase followed by a decline during odor exposure (Figures 2H and 2I), with a rebound in Ca^{2+} activity at the termination of odor exposure. We found that responses to CS^+ odor exposure were completely depressed after associative conditioning, while the CS^- responses remained unaffected, regardless of the odor used as CS^+ (Figures 2H–2J). This associative plasticity was specific to Ca^{2+} signaling during odor exposure, with little effect on Ca^{2+} signaling occurring after odor cessation; this indicates that conditioning alters input to MBOn-γ2α′1 specifically during odor exposure. In addition, this depression extended to the axon tracts of MBOn-γ2α′1 (Figures 2H and S2A), supporting the proposition that action potential propagation and MBOn-γ2α′1 output are suppressed during exposure to the learned odor, thus contributing to reduced approach behavior.

We performed additional conditioning protocols to test the hypothesis that the presence of both odor and electric shock in temporal alignment was necessary and sufficient for the MBOn-γ2α′1 depression (Figure S2B). We found that odor (CS^+) temporally aligned with shock created a similar depression with or without the CS^-, and that shock only or time by itself (no stimuli) did not produce the depression (Figures S2B and S2C). We did note an unexpected increase in the response of MBOn-γ2α′1 to odors if they were unpaired with shock or when no stimuli were given (Figures S2A, S2Bii–S2Bv, S2C, 2I, and 2J). It maybe that MBn:MBOn-γ2α′1 connectivity increases across time as a nonassociative effect. Because this trend is opposite the depression observed with CS^+/shock presentation, our conclusions on the effects of CS^+ are not altered. In addition, we found that minimal US pairing with odor (1 shock, 5-s odor) caused a weak but significant depression (Figures S2Biii and S2C), highlighting a correlation between the strength of the conditioning stimuli and MBOn-γ2α′1 plasticity. Finally, standard conditioning leads to MBOn-γ2α′1 depression that decays to nonsignificant levels by 1 hr (FiguresS2D and S2E), displaying kinetics similar to DA-mediated forgetting (Berry et al., 2012).

These data support the model that odor-activated MBn:MBOn synapses become depressed when odor-driven MBn activation is paired with US-driven activation of DAn-γ2α′1, which is similar to observations using artificial DAn activation (Hige et al., 2015; Cohn et al., 2015). Given that optogenetic stimulation of MBOn-γ2α′1 drives approach behavior (Aso et al., 2014b), this large depression in the CS^+ input compared to the CS^- would shift the MBOn network away from approach and toward avoidance during memory retrieval.

Strong Electric Shock Restores Previously Depressed MBOn-γ2α′1 Responses and Causes Forgetting

Studies in our lab and other labs have provided clear evidence that strong activation of DAns after learning causes behavioral forgetting (Berry et al., 2012, 2015; Aso and Rubin, 2016). We therefore asked whether activating DAn-γ2α′1 with strong electric shock stimuli after formation of the MBOn-γ2α′1 depression could disrupt the cellular memory trace. We exposed flies to the CS^+ (MCH) in association with either a weak (45 V, 12×) or strong US (90 V, 12×) without CS^- exposure to form the MBOn-γ2α′1 memory trace (Figure 3A). Then, we attempted to disrupt this trace with a subsequent and strong shock stimulus (150 V, 12×). We found that training with both weak and strong US stimuli produced a strong depression to the CS^+ input, with no effect on the response to a control odor (Figures 3B, 3C, S3A, and S3B). Furthermore, the strong post-learning 150-V shock stimulus significantly restored responses to the CS^+ produced by conditioning with a 45-V US. However, conditioning with a 90-V US produced an MBOn-γ2α′1 memory trace that was refractory to the 150-V post-learning stimulus (Figures 3C, S3C, and S3D). We conclude from this that the strong post-learning shock is sufficient to disrupt the memory trace produced by weak but not strong training.

To demonstrate the behavioral relevance of these physiological results, parallel memory experiments were conducted mimicking the above protocol (Figure 3D). Pairing of odor with a weak US (45 V, 12×) produced substantial aversive memory, and this performance was lost when a strong shock stimulus (150 V, 12×) was presented after learning (Figure 3E). To confirm that memory formation and its subsequent removal by the strong shock was a result of changes in behavioral response specifically to the paired odor, odor avoidance was measured in a parallel group of flies. We found that pairing an odor A (MCH) with an aversive US causes a robust increase in avoidance only to the paired odor and that this increased avoidance is completely reversed with the subsequent strong shock stimulus. Avoidance to two other odors, OCT and ethyl lactate (EL), were not altered by this MCH pairing and subsequent strong shock (Figure 3F), paralleling the memory trace changes seen in MBOn-γ2α′1.

We conclude from these results that pairing odor with a weak shock stimulus depresses subsequent MBOn-γ2α′1 responses to the learned odor and that this depression is disrupted by DAn activation through strong shock stimulation. Moreover, the odor/US$_{(weak)}$ pairing produces conditioned behavioral responses to the odor, and these responses are reversed by DAn activation through strong shock stimulation. Because the effects of strong shock were specific to the CS^+ odor and not control odors (Figures 3B, 3C, S3C, and S3D), we propose that depressed synapses are preferentially sensitive to DAn output, while other synapses in the MBn:MBOn synaptic network are less affected. Our data also indicate that strong memories, like those produced after standard conditioning with 90 V, are more resistant to DAn-mediated forgetting, while weaker memories and their memory traces are more vulnerable. This feature would allow the γ2α′1 compartment to store strongodor memories with little interference from forgetting processes, while weaker memories are removed.

New Learning Depresses Responses to New Learned Odors while Restoring Responses to Previously Learned Odors

To extend our results and further test the flexibility of this compartment to update MBn:MBOn connectivity to changing CS/US associations, we mimicked the stimulus protocols used in long-term depression/long-term potentiation (LTD/LTP) experiments in which we repeatedly measured MBOn-$\gamma2\alpha'1$ responses to two odors before, during, and after both a learning period and a forgetting period (Figure 4A). During the learning period, all of the groups received three pairings of a single US shock with short odor exposure (MCH, the CS$^+$). During forgetting, the groups were separated into one with no subsequent shock stimuli (no shock), one with three shock exposures unpaired with the CS$^+$ (unpaired 33), and one with three shock exposures unpaired with the CS$^+$ but paired with the CS$^-$ (OCT) of the learning period (reversal 33; Figure 4A). Given our results as detailed above, we anticipated that single shock pairing with brief odor presentation would create weak associations, such that a depressed CS$^+$ response of MBOn-$\gamma2\alpha'1$ to odor would be more easily disrupted by unpaired DAn-$\gamma2\alpha'1$ activation. We found that as few as three of these weak pairings were required to completely depress the response of MBOn-$\gamma2\alpha'1$ to the odor CS$^+$ (Figure 4C). This protocol also allowed us to measure MBOn-$\gamma2\alpha'1$ responses during the association (i.e., acquisition) process itself. We found that the depression appeared immediately during the first CS/US pairing (trial 3) and that this depression grew stronger with each pairing, while leaving responses to the CS$^-$ odor unaffected (Figures 4 and S4A). These data suggest that memory is both stored in and retrieved from MBn:MBOn-$\gamma2\alpha'1$ synapses immediately (within seconds) after aversive learning.

The CS$^+$-specific depression remained somewhat stable in the absence of additional shock stimuli after this learning period for at least 15 min (Figures 4B [paired→––], 4C, and S4B). We note that repeated odor exposures beyond trial 11 caused a rapid decline in responsiveness to OCT (Figures 4B [paired→–– and paired →unpaired] and 4C) or if no shocks are ever given to the animals (data not shown). This resembles the "repetition suppression" phenomenon that was recently reported for the MBOn-$\alpha'3$ (Hattori et al., 2017). Therefore, we have focused our analysis on trials 1–11. Similar to what was observed with weak 45 V, 12× learning (Figures 3B, 3C, S3C, and S3D), shock exposure unpaired with the CS$^+$ significantly restored the response of MBOn-$\gamma2\alpha'1$ to odor, with no measurable change to the CS$^-$ (trials 9–15, paired →unpaired, Figures 4B, 4C, and S4C). When the shock pulses were paired with the CS$^-$ (OCT) and unpaired with the CS$^+$, we observed the expected depression to the CS$^-$ (trials 8–10, paired →Rev, Figures 4B, 4C, and S4D), but this protocol also produced a simultaneous restoration of the CS$^+$ (MCH) responses, similar to the unpaired protocol (trials 10–15, paired→Rev, Figures 4B, 4C, and S4D). These data indicate that three pairings of a strong shock with an odor creates an immediate depression in the responsiveness of MBOn-$\gamma2\alpha'1$ that is vulnerable and easily disrupted by three subsequent and unpaired electric shocks. Furthermore, these results suggest that new learning can cause forgetting through the disruption of previously formed memory traces.

DAn-γ2α′1 Activation Alone Can Depress or Restore MBOn-γ2α′1 Responses

Electric shock, our US above, activates multiple DAns and likely many other types of neurons in the fly brain (Yu et al., 2005, 2006; Mao and Davis, 2009). While DAn-γ2α′1 is robustly activated by this type of US (Figure 2D) and is the only DAn with axonal terminals covering MBOn-γ2α′1 dendrites, we tested whether optogenetic activation of the DAn-γ2α′1 itself, in lieu of electric shock, would be sufficient to modulate MBOn-γ2α′1 connectivity. We used the red light-activated cation channel, Chrimson, fused to tdTomato (ChrT; Hoopfer et al., 2015) for this purpose. When we expressed ChrT along with GCaMP^{6f} specifically in DAn-γ2α′1 and pulsed a red-orange light-emitting diode (LED) (617 nm) onto the heads of flies through a fiber optic cable (Figures 5A and 5B), we found robust and immediate Ca^{2+} transients in the DAn synaptic terminals, while flies lacking ChrT expression in DAn-γ2α′1 showed no LED-induced activation (Figures 5C and 5D). These data indicate that short LED pulses can activate DAn-γ2α′1 with temporal precision through the head cuticle. Next, we expressed GCaMP^{6f} in the MBOn-γ2α′1 while simultaneously expressing ChrT specifically in the DAn-γ2α′1 (Figures 5E and 5F). To minimize unwanted activation of ChrT from Ca^{2+} imaging, we scanned a small section of the MBOn-γ2α′1 axon tracts outside the ChrT-enriched DAn-γ2α′1 terminals with infrared light (two-photon imaging) and sampled odors at only three time points. Mimicking the short odor-US pairing protocol used in Figure 4, we sampled the odor responses of MBOn-γ2α′1 before (pre), after a learning period (post 1), and finally after a forgetting period (post 2; Figure 5G). Similar to our results above, obtained with electric shock stimuli, pairing LED pulses with odor (MCH) led to a complete depression of CS$^+$ responses for MBOn-γ2α′1, with no effect on the CS responses (Figures 5H and 5I, paired > decay or paired > unpaired). After this initial depression, LED pulses presented unpaired with odor led to the restoration of the CS$^+$ responses of MBOn-γ2α′1, but had no effect on the CS$^-$ odor responses. There was no significant modulation of MBOn-γ2α′1 responses when no LED was presented (Figures 5H and 5I), and flies lacking ChT expression in DAn-γ2α′1 exhibited no significant depression or response restoration to the CS$^+$ odor (Figures S5A and S5B). These results indicate that output from DAn-γ2α′1 directly modulates MBOn-γ2α′1 odor responses in a bidirectional manner, presumably through MBn:MBOn synaptic connectivity, with the directionality depending on its association or lack of an association with MBn activation.

DISCUSSION

In this study, we provide several significant findings showing how neural circuits encode new memories and remove the old (Figure 6). We identify the MBn:MBOn-γ2α′1 circuit as a locus for the retrieval of short-term memory (Figure 1), likely stored as cellular memory trace formed immediately after aversive learning and manifested as a depressed activation of MBOn-γ2α′1 in response only to the paired odor (Figure 2). More important, we demonstrate that this odor-specific depression in MBOn-γ2α′1 input forms in parallel with an increase in odor avoidance only to the paired odor (Figure 3). Given that approach-driving MBOn circuits, such as MBOn-γ2α′1, antagonize MBOn circuits driving avoidance (Aso et al., 2014b), we argue that the MBOn-γ2α′1 memory trace removes this antagonism and shifts the MBOn network balance toward odor avoidance. Thus, this cellular trace

encodes a component of the aversive memory engram that drives the expression of shortterm aversive memory. As an extension, we show that behavioral forgetting induced by unpaired electric shock occurs in parallel with the disruption of the MBOn-γ2α′1 memory trace, and that both formation and disruption of this trace are controlled by the activation of DAn-γ2α′1 (Figures 3 and 5). Prior studies have primarily focused on MBOn function for behavioral output or their cellular response properties after acquisition, without addressing how cellular memory traces are affected by forgetting (Séjourné et al., 2011; Plaçais et al., 2013; Owald et al., 2015; Hige et al., 2015; Cohn et al., 2015; Perisse et al., 2016; Aso and Rubin, 2016). Our study demonstrates that a single DAn can drive the formation of a cellular memory trace during learning and its disruption during forgetting, likely through the modulation of MBn:MBOn synapses.

Recent studies in the mouse have indicated that forgetting of long-term fear memories after protein synthesis inhibition (Ryan et al., 2015) or during Alzheimer disease (Roy et al., 2016) occurs through the disruption of retrieval and not erasure of the engram. In this study, we focused on short-term aversive memory, and our data suggest that the cellular effects (i.e., a depressed odor-specific input) underlying memory encoding and its retrieval can be disrupted by DAn-mediated mechanisms after learning. These disruptions of the cellular memory trace, in turn, likely cause failure of memory retrieval, and thus forgetting. We cannot exclude the possibility that after this disruption some hidden cellular memory traces remain that may allow for the reconstitution of this memory trace at a later time, perhaps by retraining, similar to "savings" memory, originally proposed by Ebbinghaus (1885/1913). While this short-term memory trace is not long-lasting, other compartments have been implicated as loci for the storage of stable long-term memory (e.g., Séjourné et al., 2011; Aso and Rubin, 2016). Future efforts to examine how DAns alter memory traces in these compartments and the permanence of these effects should prove interesting.

We demonstrate that new learning simultaneously drives the formation of a new memory trace with the disruption of an older one (Figure 4). This probably occurs because the axon terminals of a single dopamine neuron spread broadly across the MBn:MBOn-γ2α′1 connections, such that activation of DAn-γ2α′1 would lead to the release of dopamine simultaneously across two sets of synapses—those activated by the new odor and those that are silent and depressed as part of the original engram. This feature allows the system to synchronize the disruption of weak or unimportant memories with the encoding of new more temporally relevant memories. In addition, the erosion of cellular memory traces occurring with new learning can mechanistically explain retroactive interference (Wixted, 2004). However, this observation does not imply that memories are always traded one for another. Higher intensity US (electric shock) paired with odor increased the resistance of the memory trace to DAn-based forgetting (Figure 3). While the mechanism for this resistance is unclear, this feature allows the circuit to regulate memory persistence; memory engrams that are most impactful or meaningful resist active forgetting mechanisms. Previously, we found that labile, nonconsolidated memories were most sensitive to DAn-based forgetting (Berry et al., 2012). It is possible that more impactful learning leads to MBn:MBOn synaptic alterations that are rapidly consolidated and more resistant to subsequent DA exposure.

How does the MB circuit respond to the same signal, DA, in opposing ways (i.e., forming memories or weakening them)? We hypothesized in our original study that different intracellular states at the time of DA signaling for learning and forgetting may be key (Berry et al., 2012). In agreement with that hypothesis, our present study and others (Aso et al., 2014b; Cohn et al., 2015; Hattori et al., 2017) show that MBn:MBOn synapses respond to DA in opposing ways depending on whether they are activated or are depressed at the time of DAn activation. Prior studies have shown that the coincident activation of second messenger systems—Ca^{2+} driven by odor activation of MBn and cyclic adenosine monophosphate (cAMP) driven by DA input—supports memory formation (Tomchik and Davis, 2009). Therefore, it is possible that high Ca^{2+} in combination with cAMP within odor-activated synapses drive synaptic depression, while DA signaling in a lower Ca^{2+} context in depressed synapses drives the restoration of MBn:MBOn synaptic connectivity. However, differential DA receptor signaling is also involved, with the dDA1 receptor driving learning (Kim et al., 2007; Qin et al., 2012) and the DAMB receptor driving forgetting (Berry et al., 2012). These receptors couple differentially to G proteins, with the dDA1 receptor coupling strongly to Gαs and the DAMB receptor coupling preferentially to Gαq (Himmelreich et al., 2017). Additional studies are required to connect the circuit mechanisms in the present study with second messenger system dynamics and differential DA receptor and G protein signaling to obtain a deeper understanding of memory management.

While our results indicate that DA bidirectionally modulates MBn:MBOn connectivity, it remains unclear whether this synaptic modulation is orchestrated within the MBn, the MBOn, or both neuron types. Given that the DAn synapse with MBn axons and MBOn dendrites and DA receptors reside in both compartments (Takemura et al., 2017; Hattori et al., 2017; Crocker et al., 2016), both sides of the synapse are probably modulated. However, many of the molecules required for normal memory formation and forgetting are expressed and required in MBns, including adenylyl cyclase (Mao et al., 2004), dDA1 (Qin et al., 2012), Gαs (Connolly et al., 1996), Rac1 (Shuai et al., 2010), Scribble (Cervantes-Sandoval et al., 2016), and Gαq (Himmelreich et al., 2017). Therefore, the plasticity observed here, after both learning and forgetting, likely involves some modulation of presynaptic neurotransmitter release.

Finally, our results add further evidence that an individual DAn, activated by a specific impactful stimulus, can modulate its respective MBn:MBOn circuit (Hige et al., 2015; Cohn et al., 2015). Other DAns, also responding to distinct and impactful stimuli, modulate other distinct compartments of the MBs (Boto et al., 2014; Cohn et al., 2015). The segregation of the US through parallel DAn→MBn (compartments) theoretically allows the encoding of independent cellular memory traces, or "memory bits," in parallel. However, this model is overly simplistic as several MBOns project laterally to provide synaptic input to other MBn:MBOn compartments and probably regulate the expression or stability of memory engrams stored there (Perisse et al., 2016; Shuai et al., 2015). In addition, the axon terminals of some MBOns localize in proximity to the dendrites of DAns modulating different MBn:MBOn compartments (Aso et al., 2014a). For example, MBOn-γ2α′1 potentially plays a role in the reconsolidation of reward memories formed in other MB compartments through activation of the corresponding DAns (Felsenberg et al., 2017). These inter-

compartmental circuit motifs may allow complex interactions between the memory traces stored in different compartments, including either positive or negative effects on memory stability.

STAR★METHODS

KEY RESOURCES TABLE

REAGENT or RESOURCE	SOURCE	IDENTIFIER
Antibodies		
Rabbit polyclonal anti-GFP	ThermoFischer	Cat#A11122; RRID: AB_221569
Mouse monoclonal anti-nc82	University of Iowa Developmental Studies Hybridoma Bank	RRID: AB_2314866
Mouse monoclonal anti-GFP	Sigma-Aldrich	Cat#G6539; RRID: AB_259941
Alexa 488 goat polyclonal anti-rabbit IgG	ThermoFisher	Cat#A11008; RRID: AB_143165
Alexa 633 goat polyclonal anti-mouse IgG	ThermoFisher	Cat#A21052; RRID: AB_2535719
Alexa 488 goat polyclonal anti-mouse IgG	ThermoFisher	Cat#A11029; RRID: AB_138404
Alexa 633 goat polyclonal anti-rabbit IgG	ThermoFisher	Cat#A21070; RRID: AB_2535731
Experimental Models: Organisms/Strains		
D. melanogaster: w^{1118}: w^{1118};+;+	Bloomington Drosophila Stock Center	Cat#3605
D. melanogaster: R25D01-lexA: w^{1118}; P{GMR25D01-lexA}attp40;+	Jenett et al., 2012 / Bloomington Drosophila Stock Center	Cat#53519
D. melanogaster: R13F02-gal4: w^{1118}; +; P{GMR13F02-gal4}attp2	Jenett et al., 2012 / Bloomington Drosophila Stock Center	Cat#48571
D. melanogaster: MB077B-gal4: w^{1118}, P{R25D01-p65.AD}attP40; P{R19F09-GAL4.DBD}attp2	Aso et al., 2014a / Bloomington Drosophila Stock Center	Cat#68283
D. melanogaster: MB296B-gal4: w^{1118}; P(R15B01-p65.AD}attp40; P{R26F01-GAL4.DBD}attp2	Aso et al., 2014a / Bloomington Drosophila Stock Center	Cat#68308
D. melanogaster: UAS-shi^{ts1}: w^{1118};;P{JFRC100–20XUAS-TTS-shibire(ts1)-p10}VK0005	Pfeiffer et al., 2012	N/A
D. melanogaster: UAS-GCaMP^{6f}: w^{1118}; P{20XUAS-IVS-GCaMP6f}attp40; +	Chen et al., 2013 / Bloomington Drosophila Stock Center	Cat#42747
D. melanogaster: UAS-myr::GFP: w^{1118}; +; P{10XUAS-IVS-myr::GFP}attp2	Pfeiffer et al., 2010 / Bloomington Drosophila Stock Center	Cat#32197
D. melanogaster: UAS-myr::tdTomato: w^{1118}; +; P{10XUAS-IVS-myr::tdTomato}attp2	Pfeiffer et al., 2010 / Bloomington Drosophila Stock Center	Cat#32221
D. melanogaster: lexAop-CD4::spGFP11: w^{1118}; P{lexAop-CD4::spGFP11}; +	Macpherson et al., 2015 /	N/A
D. melanogaster: UAS-syb::spGFP1–10: w^{1118}; +; P{UAS-syb::spGFP1–10}	Macpherson et al., 2015	N/A
D. melanogaster: lexAop-GCaMP^{6f}: w^{1118}; P{13XLexAop2-IVS-GCaMP6f-p10}su(Hw)attp5; +	Bloomington Drosophila Stock Center	Cat#44277
D. melanogaster: UAS-Chrimson::tdTomato (Chr): w^{1118}; +; P{20XUAS-IVS- Syn21-Chrimson::tdTomato-3.1}VK0005	Hoopfer et al., 2015	N/A

CONTACT FOR REAGENT AND RESOURCES SHARING

Further information and requests for resources and reagents should be directed to and will be fulfilled by the Lead Contact, Ronald Davis (rdavis@scripps.edu).

EXPERIMENTAL MODEL AND SUBJECTS DETAILS

Fly Conditions and Strains—Fly stocks were cultured on standard food at room temperature. Crosses were raised on standard food at 25°C with 70% relative humidity and a 12-hr light-dark cycle for all experiments with the following exceptions. Crosses used for shibire[ts1] experiments were raised at 18°C until 2 days post eclosion and then progeny were maintained at 23°C for 1 day prior to olfactory conditioning and memory tests (see below). Crosses used for optogenetic experiments were kept on standard food at 25°C with 70% relatively humidity but kept in the dark using aluminum foil until 2 days post eclosion, when progeny were transferred in dim blue light to food vials containing all-trans-retinal (0.5 mM, Sigma-Aldrich, cat #R2500) and continually maintained in the dark via foil for 3–4 days until imaging. Flies were generally 3–6 days old at the time of behavioral, *in vivo* imaging, immunostaining and GRASP assays. For all olfactory behavior assays, mixed gender populations of flies (50–60 flies housed per vial) were used, whereas only females (16 flies housed per vial) were used for *in vivo* imaging, immunostaining confocal, and SIM experiments. The following lines were used for experiments, crosses, and to generate stocks: w^{1118}; *R25D01-lexA* in *attP40* (Jenett et al., 2012); *R13F02-gal4* in *attP2* (Jenett et al., 2012); *MB077B* split *gal4* consisting of *R25D01-p65.AD* in *attP40* and *R19F09-GAL4.DBD* in *attP2* (Aso et al., 2014a); *MB296B* split *gal4* consisting of *R15B01-p65.AD* in *attP40* and *R26F01-GAL4.DBD* in *attP2* (Aso et al., 2014a); *20XUAS-shibire[ts1]* in *VK0005* (Pfieffer et al., 2012, a gift from Gerry Rubin); *20XUAS-IVS-GCaMP[6f]* in *attP40* (Chen et al., 2013); *10XUAS-IVS-myr::GFP* in *attP2* (Pfeiffer et al., 2010); *10XUAS-IVS-myr::tdTomato* in *attP2* (Pfeiffer et al., 2010); *lexAop-CD4::spGFP[11]* in 2nd chromosome (Bloomington *Drosophila* Stock Center); *UAS-syb::spGFP[1–10]* in 3rd chromosome (Macpherson et al., 2015); *13XLexAop2-IVS-GCaMP[6f]-p10* in su(Hw)attP5 (Bloomington *Drosophila* Stock Center); *20XUAS-IVS-Syn21-Chrimson::tdTomato-3.1* in *VK0005* (Hoopfer et al., 2015).

METHOD DETAILS

Immunostaining and GRASP—For immunostaining of GFP expression driven by MB077B-gal4 (Figure 1C and S1A), whole brains were isolated and processed similar to the Fly Light Project protocol (Janelia Research Campus, Jenett et al., 2012). Specifically, adult brains were isolated from the head in ice cold S2 medium (ThermoFisher, cat #21720–024), transferred into 1% paraformaldyhyde (PFA) in S2 medium, and nutated overnight at 4°C. After 3 washes consisting of incubation in PAT3 medium (0.5% Triton X-100, 0.5% bovine serum albumin, in phosphate buffered saline) for 1 hr at room temperature with nutation, brains were incubated in normal goat serum (3%) for 1.5 hr at room temperature on nutator. Brains were then incubated with primary antibodies for 3 hr at room temperature and then overnight at 4°C. After another 3× wash with PAT3 medium (as above), brains were incubated with secondary antibodies for 3 hr at room temperature followed by 5 days at 4°C. Brains were washed once again in PAT3 medium 3 times, once in 1X PBS, and then placed on slides between spacers (102 μm) in VectaShield mounting medium, covered with a coverslip, and sealed with clear nail polish. Images were collected using a 10X objective with a Leica TCS SP5 Confocal microscope with 488 and 633 laser excitation. The step size for z stacks was 1 μm with images collected at 512×512 pixel resolution. Primary

antibodies used: rabbit polyclonal anti-GFP (1:1000, ThermoFisher, cat# A11122) and mouse monoclonal anit-nc82 (1:50, Developmental Studies Hybridoma Bank, AB2314866). Secondary antibodies used include: goat polyclonal ant-rabbit IgG conjugated to Alexa Fluor 488 (1:800, ThermoFisher, cat# A11008), goat polyclonal anti-mouse IgG conjugated to Alexa Fluor 633 (1:400, ThermoFisher, cat# A21052). For structured illumination microscopy (SIM, Figure 1D and S1C), brains were processed as above, except after the last 3 PAT3 washes, brains were washed in PBS then quickly rinsed in dH_2O and mounted on poly-lysine coated high-precision coverslips. Samples were then dehydrated using an ethanol series (20%, 30%, 50%, 70%, 95%, 100% x2, 5min each), cleared in methyl salicylate overnight and mounted (as above) in methyl salicylate. Samples were imaged using a Zeiss ELYRA PS1, 63× oil emersion objective, with 488 nm and 642 nm laser excitation. Primary antibodies used for SIM: mouse moncolonal anti-GFP (specific to fully reconstituted GFP referred to as "α-GRASP" in manuscript, 1:1000, Sigma-Aldrich, cat# G6539) and rabbit polyclonal anti-GFP (specific for spGFP[1−10] fragment referred to as "α-syb::spGFP[1−10]," 1:1000, Invitrogen, cat #A11122). Secondary antibodies used include: goat polyclonal anti-mouse IgG conjugated to Alexa Fluor 488 (1:800, Invitrogen, cat# A11029), goat polyclonal anti-rabbit IgG conjugated to Alexa Fluor 633 (1:400, Invitrogen, cat# A21070). For native GRASP experiments (Figure S1B), brains were dissected in physiological saline (see "Mounting and Dissecting Flies for Imaging" for recipe) and attached to the bottom of a Petri dish. Images were acquired at 1 μm z steps using a 25X immersion objective with a Leica TCS SP8 Confocal microscope and a 488 nm Argon laser.

Olfactory Conditioning—Olfactory associative conditioning was conducted in a way similar to standard olfactory conditioning (Beck et al., 2000) (Figure 1E,F) and then flies were subsequently tested in a T-maze assay (see "Odor Avoidance and Memory Tests" for details of testing procedure). For conditioning, groups of 50–60 flies were first equilibrated for > 15 min in fresh food vials in a training room dimly lit with red light and 65%–75% humidity, and were then loaded into a training tube where they were exposed to 30 s of fresh air, 1 min of an odor (the CS+) paired with 12 electric shock pulses (1.25 s duration, 90V delivered through electrified shock grids, every 5 s), 30 s of fresh air, then 1 min of the odor not paired with electric shock (the CS-), and finally followed by 30 s of fresh air. The electric shocks began 3.75 s after the start of the CS+. Flies were then transferred to fresh food vials for subsequent testing. For single odor conditioning (Figure 3D-F), flies were treated as above except 45V was used to pair with the CS+, and the CS- odor was omitted. After conditioning, flies were maintained at 23–25°C for the single odor conditioning experiments (Figure 3D-F). For synaptic blockade experiments throughout memory (Figure 1E), flies were either tapped into either 23°C or 32°C food vials, 15 min prior to acquisition and retrieval. For blocking synaptic output only during retrieval (Figure 1F), flies were tapped into 18°C food vials 15 min prior to acquisition. The flies were immediately tapped back into 18°C food vials after conditioning and then moved to 27°C or kept at 18°C for ~3.5 min prior to retrieval. Flies were treated with a lower restrictive temperature (27°C) for retrieval experiments because preliminary data (not shown) demonstrated that treating flies to high temperature (32°C) immediately after acquisition significantly disrupted performance of control flies, potentially due to heat stress. Flies for memory tests (Figure 1E,F or Figure 3E) were conditioned using either MCH (4-methylcyclohexonal) or OCT (3-

octanol) as the CS+ at concentrations of 0.05%–0.07% and 0.05%–0.08% in mineral oil, respectively.

After single odor conditioning (Figure 3D-F), starting at 5.5 min after the associative conditioning, two groups of flies were transferred into an additional set of clean conditioning tubes, one (Paired A) received 1 min of fresh air and a second (Paired A - > 150V stim) received 1 min of fresh air with 12×, 150V electric shocks (same duration and spacing as during associative conditioning but unpaired with test odors). All groups were then tested 8.5 min after aversive conditioning for their preference between the CS+ odor and the second odor (i.e., if MCH is CS+, then OCT is second odor). Flies for odor avoidance tests (Figure 3F) were conditioned as above using only MCH as a CS+ (0.04% in mineral oil). Like the described memory tests, these flies were divided into "Paired A" and "Paired A -> 150V" groups and treated like above. These groups were compared to a "naïve" odor avoidance group that received no conditioning (no exposure to test odors or electric shock) prior to the odor avoidance test.

Odor Avoidance and Memory Tests—To test olfactory memory (Figure 1E,F and 3E), two groups of flies conditioned (see "Olfactory Conditioning" above) to either MCH or OCT as the CS+ were transferred into two T-mazes (1 vial of 50–60 per maze), given 1 min to acclimate, then given 2 min to choose between an arm with the CS+ odor and an arm with the CS- odor. Each maze gave a half performance index (half PI): Half PI = ((# flies in CS- arm) – (# flies in CS+ arm)) / (# flies in both arms). The final PI was calculated by averaging the two groups half PI's. Odor concentrations (0.05%–0.07% MCH or 0.05%–0.08% OCT in mineral oil) were chosen such that flies naive to both odors produce a PI~0. To test odor avoidance behavior for naive w[1118] flies (Figure 3F), naive flies or flies conditioned to MCH as the CS+ (Figure 3F), flies were treated as in the memory tests above, except flies chose between an arm with fresh air (air bubbled through odor-less mineral oil) and one with an odor, either MCH (the CS+ in conditioned experiments), OCT, or EL. Since there is only one odor during the choice, each maze provided an avoidance index (AI): AI = ((# flies in fresh air arm) – (# flies in odor arm)) / (# flies in both arms). Because normal memory test odor concentrations are strongly aversive, odor concentrations during the odor avoidance tests were reduced (0.025%–0.04% MCH, 0.005%–0.01% OCT, 0.025% EL) such that the AI of naive animals was around 0.2 to 0.3 to avoid ceiling level effects and make the assay sensitive to odor driven behavioral changes in both directions. The final AI was a function of flies making many behavioral choices when entering the odor arm and ultimately depends on a balance between odor driven approach and avoidance behaviors.

Mounting and Dissecting Flies for Imaging—We designed a custom setup to attach a fly without anesthesia to a "fly platform" allowing the confocal imaging of the brain immersed in physiological saline, while keeping the majority of the fly dry and completely exposed to receive odors and electric shocks (Figure 2A, similar to Berry et al., 2015). The design of this custom setup is available upon request from the authors. First, non-anesthetized flies were gently aspirated head first into a pipette tip (200 μl) cut to a diameter slightly larger than the fly thorax until the head is exposed, but not the front legs. Melted myristic acid was applied to the proboscis to secure it and prevent movement of the brain

during imaging. Flies were then gently aspirated into a slot (hand carved to snuggly fit and constrain the fly) in a plastic "fly mounting" piece that was attached to a brass "fly platform" via machine screws. The fly was gently adjusted until the head cuticle and thorax were positioned in x,y,z to align with a hole in a stainless steel shim glued to the fly platform. Viscous UV activated glue (Fotoplast, Dreve) was carefully applied around the entire interface of the fly and the shim edge, but the head cuticle was left uncovered, to ensure a watertight seal. The glue was applied and cured with a UV gun (ELC-41, Electro-lite) piecemeal in 3 sessions: the first 2 sessions using 4 s UV light pulses and the final session using 10 s of UV light pulse. The top surface of the platform/shim/fly head was washed briefly with clean water to remove excess glue. To remove the plastic mounting piece, the setup was rested upside down and pressure was applied to the corners of the plastic piece (to prevent movement laterally that would damage the glued fly) and the screws were loosened until free of the brass platform. Then the plastic piece was very carefully removed, while visually inspecting that the fly was not crushed or damaged in the process, revealing the fly glued to the platform. The fly was flailing its legs vigorously, looked healthy, and the 3rd antennal segment was dry and free of glue before proceeding. The fly platform was placed in a 3D printed holder to dissect the head cuticle. The head was covered with fresh physiological saline (124 mM NaCl, 3 mM KCl, 20 mM MOPS, 1.5 mM $CaCl_2$, 4 mM $MgCl_2$, $6H_2O$, 5 mM $NaHCO_3$, 1 mM NaH_2PO_4, H_2O, 10 mM trehalose, 7 mM sucrose, 10 mM glucose, pH 7.2) and the head cuticle, fat bodies, and trachea above the brain were removed. One ml of physiological saline was used for all experiments except the 1 hr post associative conditioning experiments (Figure S1D-E), where the longer time commanded continuous 1 ml/ min perfusion.

***In Vivo* Imaging Microscope Conditions**—For imaging GCaMP[6f] fluorescence with single photon excitation we used a Leica TCS SP5 II confocal microscope. A 488 nm Argon laser (with variable power, see below) was line scanned (8000 hz, resonant frequency) at a resolution of 512×512 pixels using a 20X objective (HCX APO L 20.0X/1.0NA, Leica) at a frame rate of 2Hz with the pinhole fully open. Emitted light was collected using a PMT (510–600 nm) for GCaMP emission and a second PMT (600–700nm) for tdTomato emission. The laser power was adjusted to deliver 20–30 μW at the objective. In order to limit unwanted activation of DAn-γ2α'1 expressing Chrimson, a channel sensitive to light across the visible spectrum (Klapoetke et al., 2014), we utilized 2-photon imaging with a Leica TCS SP8 confocal microscope with an infrared laser tuned to 920 nm. These experiments were conducted with the above single photon conditions but with some exceptions. Laser light was line scanned (700 hz) at a resolution of 256×256 pixels. For imaging GCaMP[6f] in DAn-γ2α'1 w or w/o Chrimson expression (Figure 5A-D), we used a laser power of ~35 mW at the objective and emitted light was collected using a HyD detector (460–570 nm) for GCaMP emission and PMT (600–700nm) for tdTomato. For imaging GCaMP[6f] in MBOn-γ2α'1 w or w/o Chrimson expression in the DAn-γ2α'1 (Figure 5G-I), low GCaMP[6f] expression with *R25D01-lexA* required higher laser power (~115 mW at the objective) and emitted light was collected using a HyD detector (460–570 nm) for GCaMP emission and PMT (600–700nm) for tdTomato. In order to take additional steps to limit activation of Chrimson during GCaMP imaging, we scanned only a region (ROI scan) of the MBOn-γ2α'1 axon exiting the MBs where little Chrimson enriched DAn-

γ2α'1 terminals were located (as reported by tdTomato signal, see Figure 5F). Second, the 920 nm laser light was applied to the brain to record responses to both odors at only 3 time windows (Pre, Post 1, Post 2, illustrated in Figure 5G) by opening and closing the shutter during the recording. For each odor response time window, the shutter was opened ~20 s prior to a 5 s odor exposure and closed 5 s after the odor ended.

Stimulus Delivery for *In Vivo* Imaging—To deliver odors to flies under the microscope, a small stream of air (100 ml/min) was diverted (via solenoids) from flowing through a clean 20 mL glass vial to instead flow through a 20 mL glass vial containing a 0.5 μL drop of pure odorant. This air stream was then serial diluted into a larger air stream (1000 ml/min) before traveling 95 cm through Teflon tubing (~2.5 mm diameter) to reach the fly. To deliver shocks to flies under the microscope, a costume shock platform was made from shock grids used in standard olfactory memory assays that consist of alternating ± charged copper strips attached to an epoxy sheet. To simulate shock exposure given during the standard olfactory memory assay, the surface of the shock platform was positioned so that all 6 legs are touching but the fly could temporarily break contact by moving its legs. To optogenetically activate DAn-γ2α'1 (Figure 5 and S5), light emitted by a redorange LED (617 nm, Luxeon, cat # SP-01-E4) was focused through an optic lens (Luxeon, cat # 10356) into a fiber optic cable (Edmund Optics, cat # 57097) and directed to the side of the head of the fly.

Odor-Shock Protocols for *In Vivo* Imaging—For odor-shock imaging experiments the following experiments were conducted after mounting flies (see above), and are listed here in order they appear in manuscript. First, to measure DAn-γ2α'1 activation in response to our standard shock protocol (Figure 2B,C), flies were imaged before, during, and after 12 electric shock pulses (90V). The duration and spacing of shock pulses were identical to that given during "Olfactory Conditioning" above. With MBOn-γ2α'1 GCaMP experiments, we quantitated the Ca^{2+} based responsiveness of MBOn-γ2α'1 before, during, and after 5 s odor pulses. We initially quantitated the responsiveness at a given time point (i.e, "Pre," "Post 1," "Post 2," Figures 2 and 3) by exposing the fly to a probe sequence of two odors, two times, with the odor type interleaved and with a 30 s inter-pulse interval (i.e., MCH- > OCT- > MCH- > OCT). For a given group of animals, both odor sequences (i.e., MCH first or OCT first) were given in equal numbers then pulses for each odor type were averaged to give one average "activity" dataset across time for each odor (see "Quantification and Statistical Analysis"). For our initial associative memory experiments (Figure 2E-J), after initial "Pre" stimuli, we exposed flies to the exact protocol (see timeline in Figure 2G) used for "Olfactory Conditioning" (see Paired in Figure 2G). As a control with the same stimuli but without the temporal contiguity of the CS+ and US, we included an Unpaired group in which the electric shock was moved to finish 3 min ahead of the CS+ odor exposure. Both Paired and Unpaired groups were split into those where during conditioning the first odor ("A") was MCH and the second odor ("B") was OCT, or vice versa, and all protocols ended with a Post probe sequence. Experiments aimed at reducing down the essential stimuli required to produce a depressed MBOn response (Figure S2B,C) followed the same timeline as Paired and Unpaired (Figure 2E-J) except "ii) CS+ only" lacked the CS-, "iii) CS + (1shock)" was a 5 s odor pulse with 1.25 s 90V shock pulse starting 1 s after odor start,

"iv) Shock only" lacked both CS+ and CS-, and "v) No stimuli" lacked both odors and electric shock. For 1 hr odor memory trace experiments (Figure S2D-E), the Post probe sequence was moved to 1 hr after the CS- ended. For single odor conditioning during imaging (Figure 3D-F and S3A-D) we followed the same odor/shock treatment as with single odor condition for behavioral memory assays (see "Olfactory conditioning," Figure 3E,F), such that the time between the start of the CS+/shock exposure and the Post 2 probe sequence was equivalent to the time between conditioning and T-maze tests of the behavioral assays. For short odor pulse conditioning experiments involving shock (Figure 4 and S4), we probed the responsiveness of MBOn-γ2α'1 to each odor by giving 5 s of MCH followed by 5 s of OCT with a 45 s inter pulse interval, and repeated this sequence for 15 trials. During the learning phase (trials 3–5), a 90V electric shock (3 s duration) was given following the MCH odor pulse by ~1 s. For Unpaired (paired- > unpaired) animals, the subsequent 90V electric shock (3 s duration) started 22 s prior to the MCH odor pulse from trials 8–10. For Reversal (paired- > Rev) animals, the subsequent electric shock started 1 s after the start of the OCT odor pulse from trials 7–9.

Optogenetic Protocols for *In Vivo* Imaging—We performed optogenetic imaging experiments in a dark room and mounted/dissected flies using only dim blue light to prevent Chrimson mediated activation of DAn-γ2α'1. After mounting flies (see above) and focusing the confocal on the neural structure to be imaged, we waited 5 min before beginning experimental recordings to allow time for recovery from any unwanted DAn-γ2α'1 activation that occurred while finding the brain region of interest. To measure DAn-γ2α'1 activation in response to LED light exposure (Figure 5A-C), GCaMP[6f] was expressed using *MB296B-gal4* with or without co-expression of Chrimson::tdTomato, and fluorescence was imaged before and after 6 LED pulses (see "Stimulus Delivery for In Vivo Imaging") of either 1 or 5 msec duration given at 2 hz frequency. For experiments in which we activated DAn-γ2α'1 while imaging odor responsiveness of MBOn-γ2α'1 (Figure 5G-I and S5), short odor pulse conditioning (as described in "Odor-Shock Protocols for In Vivo Imaging") was performed but, in lieu of electric shock, 6 LED pulses of 1 msec duration (2 hz frequency) were given 1 s after the start of the MCH pulses from trials 3–5 (Paired > Decay and Paired > Unpaired) and also again starting 22 s before MCH pulses from trials 8–10 (Paired > Unpaired).

Quantification and Statistical Analyses—During behavioral tests for memory and odor avoidance, the performance and avoidance indices (PI and AI, respectively) were quantified as mentioned above in "Odor Avoidance and Memory Tests" (Figures 1E,F and 3E,F). To measure neural activity during imaging experiments, we first used ImageJ to quantify GCaMP fluorescence (F) within neurons across time. For single photon imaging of MBOn-γ2α'1 (Figures 2E-J, 3A-C, 4 and S2–4), a region of interest (ROI) was drawn around the GCaMP raw F in dendrites (within the MBs) and/or the axon tract (leaving the MBs) of MBOn-γ2α'1 using a time-averaged image of the whole recording. The same was done when imaging axon terminals of DAn-γ2α'1 (Figures 2B-D and 5A-D). In the case where MBOn-γ2α'1 axon tract was ROI scanned (Figure 5E-I), the GCaMP F of the entire scanned region was quantified. The average GCaMP F within the ROI is then quantified across time. We then used MATLAB to quantify the MBOn-γ2α'1 neural "activity" across

time (t), by normalizing the GCaMP F signal to the mean signal (F_o) within 5 s prior to the start of an odor pulse as follows:

$$\text{Activity}\left(\%\Delta F/F_o\right)(t) = 100 * \left(\left(F(t) - F_o\right)/F_o\right).$$

Due to robust ongoing Ca^{2+} transients in DAn-γ2α'1 (Berry et al., 2012; 2015), we quantified its activity using this exact function except normalizing instead to the local minimum signal (F_{min}) within 5 s prior to the start of the electric shock (Figure 2D) or LED (Figure 5C) stimulus. To quantify the "Mean response" of MBOn-γ2α'1 to odors (or DAn-γ2α'1 to electric shock or LED exposure), we calculated the average of the "activity" trace during the stimulus. We then averaged these "Mean response" values across all animals in a group (plotted as the mean ± standard error of the mean) prior to statistical analysis. "Response change" (% F/F$_o$) across time (Figure S3A,C) was calculated by subtracting "activity" traces during exposure to an odor at one time point from another time point within animal (i.e., Post 1 – Pre). "Mean change" is the average of the "Response change" during the 5 s odor exposure. Statistics were performed using Prism 5 (Graphpad). All tests were two tailed and confidence levels were set at α = 0.05. Non-parametric tests were used for *in vivo* imaging data, while parametric tests were used for olfactory memory (PI) and odor avoidance (AI) comparisons as these values are normally distributed (Tully et al., 1994). The exact statistical tests used are listed in the figure legends.

Supplementary Material

Refer to Web version on PubMed Central for supplementary material.

ACKNOWLEDGMENTS

REFERENCES

Aso Y, and Rubin GM (2016). Dopaminergic neurons write and update memories with cell-type-specific rules. eLife 5, e16135. [PubMed: 27441388]

Aso Y, Hattori D, Yu Y, Johnston RM, Iyer NA, Ngo TT, Dionne H, Abbott LF, Axel R, Tanimoto H, and Rubin GM (2014a). The neuronal architecture of the mushroom body provides a logic for associative learning. eLife 3, e04577. [PubMed: 25535793]

Aso Y, Sitaraman D, Ichinose T, Kaun KR, Vogt K, Belliart-Gue´rin G, Plac¸ais PY, Robie AA, Yamagata N, Schnaitmann C, et al. (2014b). Mushroom body output neurons encode valence and guide memory-based action selection in Drosophila. eLife 3, e04580. [PubMed: 25535794]

Beck CD, Schroeder B, and Davis RL (2000). Learning performance of normal and mutant Drosophila after repeated conditioning trials with discrete stimuli. J. Neurosci 20, 2944–2953. [PubMed: 10751447]

Berry JA, Cervantes-Sandoval I, Nicholas EP, and Davis RL (2012). Dopamine is required for learning and forgetting in Drosophila. Neuron 74, 530–542. [PubMed: 22578504]

Berry JA, Cervantes-Sandoval I, Chakraborty M, and Davis RL (2015). Sleep facilitates memory by blocking dopamine neuron-mediated forgetting. Cell 161, 1656–1667. [PubMed: 26073942]

Boto T, Louis T, Jindachomthong K, Jalink K, and Tomchik SM (2014). Dopaminergic modulation of cAMP drives nonlinear plasticity across the Drosophila mushroom body lobes. Curr. Biol 24, 822–831. [PubMed: 24684937]

Bouzaiane E, Trannoy S, Scheunemann L, Placˏ ais PY, and Preat T (2015). Two independent mushroom body output circuits retrieve the six discrete components of Drosophila aversive memory. Cell Rep. 11, 1280–1292. [PubMed: 25981036]

Busto GU, Cervantes-Sandoval I, and Davis RL (2010). Olfactory learning in Drosophila. Physiology (Bethesda) 25, 338–346. [PubMed: 21186278]

Campbell RA, Honegger KS, Qin H, Li W, Demir E, and Turner GC (2013). Imaging a population code for odor identity in the Drosophila mushroom body. J. Neurosci 33, 10568–10581. [PubMed: 23785169]

Cervantes-Sandoval I, Chakraborty M, MacMullen C, and Davis RL (2016). Scribble scaffolds a signalosome for active forgetting. Neuron 90, 1230–1242. [PubMed: 27263975]

Cervantes-Sandoval I, Phan A, Chakraborty M, and Davis RL (2017). Reciprocal synapses between mushroom body and dopamine neurons form a positive feedback loop required for learning. eLife 6, e23789. [PubMed: 28489528]

Chen TW, Wardill TJ, Sun Y, Pulver SR, Renninger SL, Baohan A, Schreiter ER, Kerr RA, Orger MB, Jayaraman V, et al. (2013). Ultrasensitive fluorescent proteins for imaging neuronal activity. Nature 499, 295–300. [PubMed: 23868258]

Claridge-Chang A, Roorda RD, Vrontou E, Sjulson L, Li H, Hirsh J, and Miesenbö ck G (2009). Writing memories with light-addressable reinforcement circuitry. Cell 139, 405–415. [PubMed: 19837039]

Cohn R, Morantte I, and Ruta V (2015). Coordinated and compartmentalized neuromodulation shapes sensory processing in Drosophila. Cell 163, 1742–1755. [PubMed: 26687359]

Connolly JB, Roberts IJ, Armstrong JD, Kaiser K, Forte M, Tully T, and O'Kane CJ (1996). Associative learning disrupted by impaired Gs signaling in Drosophila mushroom bodies. Science 274, 2104–2107. [PubMed: 8953046]

Crocker A, Guan XJ, Murphy CT, and Murthy M (2016). Cell-type-specific transcriptome analysis in the Drosophila mushroom body reveals memory-related changes in gene expression. Cell Rep. 15, 1580–1596. [PubMed: 27160913]

Davis RL (1993). Mushroom bodies and Drosophila learning. Neuron 11, 1–14. [PubMed: 8338661]

Davis RL, and Zhong Y (2017). The biology of forgetting-a perspective. Neuron 95, 490–503. [PubMed: 28772119]

Ebbinghaus H (1885/1913). Memory. A Contribution to Experimental Psychology (Teachers College, Columbia University).

Felsenberg J, Barnstedt O, Cognigni P, Lin S, and Waddell S (2017). Reevaluation of learned information in Drosophila. Nature 544, 240–244. [PubMed: 28379939]

Hattori D, Aso Y, Swartz KJ, Rubin GM, Abbott LF, and Axel R (2017). Representations of novelty and familiarity in a mushroom body compartment. Cell 169, 956–969.e17. [PubMed: 28502772]

Heisenberg M (2003). Mushroom body memoir: from maps to models. Nat. Rev. Neurosci 4, 266–275. [PubMed: 12671643]

Hige T, Aso Y, Modi MN, Rubin GM, and Turner GC (2015). Heterosynaptic plasticity underlies aversive olfactory learning in Drosophila. Neuron 88, 985–998. [PubMed: 26637800]

Himmelreich S, Masuho I, Berry JA, MacMullen C, Skamangas NK, Martemyanov KA, and Davis RL (2017). Dopamine receptor DAMB signals via Gq to mediate forgetting in Drosophila. Cell Rep. 21, 2074–2081. [PubMed: 29166600]

Hoopfer ED, Jung Y, Inagaki HK, Rubin GM, and Anderson DJ (2015). P1 interneurons promote a persistent internal state that enhances inter-male aggression in Drosophila. eLife 4, e11346. [PubMed: 26714106]

Jenett A, Rubin GM, Ngo TT, Shepherd D, Murphy C, Dionne H, Pfeiffer BD, Cavallaro A, Hall D, Jeter J, et al. (2012). A GAL4-driver line resource for Drosophila neurobiology. Cell Rep. 2, 991–1001. [PubMed: 23063364]

Kim YC, Lee HG, and Han KA (2007). D1 dopamine receptor dDA1 is required in the mushroom body neurons for aversive and appetitive learning in Drosophila. J. Neurosci 27, 7640–7647. [PubMed: 17634358]

Kitamoto T (2001). Conditional modification of behavior in Drosophila by targeted expression of a temperature-sensitive shibire allele in defined neurons. J. Neurobiol 47, 81–92. [PubMed: 11291099]

Klapoetke NC, Murata Y, Kim SS, Pulver SR, Birdsey-Benson A, Cho YK, Morimoto TK, Chuong AS, Carpenter EJ, Tian Z, et al. (2014). Independent optical excitation of distinct neural populations. Nat. Methods 11, 338–346. [PubMed: 24509633]

Lin S, Owald D, Chandra V, Talbot C, Huetteroth W, and Waddell S (2014). Neural correlates of water reward in thirsty Drosophila. Nat. Neurosci 17, 1536–1542. [PubMed: 25262493]

Liu C, Placais PY, Yamagata N, Pfeiffer BD, Aso Y, Friedrich AB, Siwanowicz I, Rubin GM, Preat T, and Tanimoto H (2012). A subset of dopamine neurons signals reward for odour memory in Drosophila. Nature 488, 512–516. [PubMed: 22810589]

Macpherson LJ, Zaharieva EE, Kearney PJ, Alpert MH, Lin TY, Turan Z, Lee CH, and Gallio M (2015). Dynamic labelling of neural connections in multiple colours by trans-synaptic fluorescence complementation. Nat. Commun 6, 10024. [PubMed: 26635273]

Mao Z, and Davis RL (2009). Eight different types of dopaminergic neurons innervate the Drosophila mushroom body neuropil: anatomical and physiological heterogeneity. Front. Neural Circuits 3, 5. [PubMed: 19597562]

Mao Z, Roman G, Zong L, and Davis RL (2004). Pharmacogenetic rescue in time and space of the rutabaga memory impairment by using Gene-Switch. Proc. Natl. Acad. Sci. USA 101, 198–203. [PubMed: 14684832]

Owald D, Felsenberg J, Talbot CB, Das G, Perisse E, Huetteroth W, and Waddell S (2015). Activity of defined mushroom body output neurons underlies learned olfactory behavior in Drosophila. Neuron 86, 417–427. [PubMed: 25864636]

Perisse E, Owald D, Barnstedt O, Talbot CB, Huetteroth W, and Waddell S (2016). Aversive learning and appetitive motivation toggle feed-forward inhibition in the Drosophila mushroom body. Neuron 90, 1086–1099. [PubMed: 27210550]

Pfeiffer BD, Ngo TT, Hibbard KL, Murphy C, Jenett A, Truman JW, and Rubin GM (2010). Refinement of tools for targeted gene expression in Drosophila. Genetics 186, 735–755. [PubMed: 20697123]

Pfeiffer BD, Truman JW, and Rubin GM (2012). Using translational enhancers to increase transgene expression in Drosophila. Proc. Natl. Acad. Sci. USA 109, 6626–6631. [PubMed: 22493255]

Placais PY, Trannoy S, Isabel G, Aso Y, Siwanowicz I, Belliart-Guérin G, Vernier P, Birman S, Tanimoto H, and Preat T (2012). Slow oscillations in two pairs of dopaminergic neurons gate long-term memory formation in Drosophila. Nat. Neurosci 15, 592–599. [PubMed: 22366756]

Placais PY, Trannoy S, Friedrich AB, Tanimoto H, and Preat T (2013). Two pairs of mushroom body efferent neurons are required for appetitive long-term memory retrieval in Drosophila. Cell Rep. 5, 769–780. [PubMed: 24209748]

Qin H, Cressy M, Li W, Coravos JS, Izzi SA, and Dubnau J (2012). Gamma neurons mediate dopaminergic input during aversive olfactory memory formation in Drosophila. Curr. Biol 22, 608–614. [PubMed: 22425153]

Richards BA, and Frankland PW (2017). The persistence and transience of memory. Neuron 94, 1071–1084. [PubMed: 28641107]

Roy DS, Arons A, Mitchell TI, Pignatelli M, Ryan TJ, and Tonegawa S (2016). Memory retrieval by activating engram cells in mouse models of early Alzheimer's disease. Nature 531, 508–512. [PubMed: 26982728]

Ryan TJ, Roy DS, Pignatelli M, Arons A, and Tonegawa S (2015). Memory. Engram cells retain memory under retrograde amnesia. Science 348, 1007–1013. [PubMed: 26023136]

Schwaerzel M, Monastirioti M, Scholz H, Friggi-Grelin F, Birman S, and Heisenberg M (2003). Dopamine and octopamine differentiate between aversive and appetitive olfactory memories in Drosophila. J. Neurosci 23, 10495–10502. [PubMed: 14627633]

Se´journe´ J, Plac¸ais PY, Aso Y, Siwanowicz I, Trannoy S, Thoma V, Tedjakumala SR, Rubin GM, Tche´nio P, Ito K, et al. (2011). Mushroom body efferent neurons responsible for aversive olfactory memory retrieval in Drosophila. Nat. Neurosci 14, 903–910. [PubMed: 21685917]

Shuai Y, Lu B, Hu Y, Wang L, Sun K, and Zhong Y (2010). Forgetting is regulated through Rac activity in Drosophila. Cell 140, 579–589. [PubMed: 20178749]

Shuai Y, Hirokawa A, Ai Y, Zhang M, Li W, and Zhong Y (2015). Dissecting neural pathways for forgetting in Drosophila olfactory aversive memory. Proc. Natl. Acad. Sci. USA 112, E6663–E6672. [PubMed: 26627257]

Sitaraman D, Aso Y, Jin X, Chen N, Felix M, Rubin GM, and Nitabach MN (2015). Propagation of homeostatic sleep signals by segregated synaptic microcircuits of the Drosophila mushroom body. Curr. Biol 25, 2915–2927. [PubMed: 26455303]

Takemura SY, Aso Y, Hige T, Wong A, Lu Z, Xu CS, Rivlin PK, Hess H, Zhao T, Parag T, et al. (2017). A connectome of a learning and memory center in the adult Drosophila brain. eLife 6, e26975. [PubMed: 28718765]

Tanaka NK, Tanimoto H, and Ito K (2008). Neuronal assemblies of the Drosophila mushroom body. J. Comp. Neurol 508, 711–755. [PubMed: 18395827]

Tomchik SM, and Davis RL (2009). Dynamics of learning-related cAMP signaling and stimulus integration in the Drosophila olfactory pathway. Neuron 64, 510–521. [PubMed: 19945393]

Tully T, Preat T, Boynton SC, and Del Vecchio M (1994). Genetic dissection of consolidated memory in Drosophila. Cell 79, 35–47. [PubMed: 7923375]

Turner GC, Bazhenov M, and Laurent G (2008). Olfactory representations by Drosophila mushroom body neurons. J. Neurophysiol 99, 734–746. [PubMed: 18094099]

Wixted JT (2004). The psychology and neuroscience of forgetting. Annu. Rev. Psychol 55, 235–269. [PubMed: 14744216]

Yamazaki D, Hiroi M, Abe T, Shimizu K, Minami-Ohtsubo M, Maeyama Y, Horiuchi J, and Tabata T (2018). Two parallel pathways assign opposing odor valences during Drosophila memory formation. Cell Rep. 22, 2346–2358. [PubMed: 29490271]

Yu D, Keene AC, Srivatsan A, Waddell S, and Davis RL (2005). Drosophila DPM neurons form a delayed and branch-specific memory trace after olfactory classical conditioning. Cell 123, 945–957. [PubMed: 16325586]

Yu D, Akalal DB, and Davis RL (2006). Drosophila alpha/beta mushroom body neurons form a branch-specific, long-term cellular memory trace after spaced olfactory conditioning. Neuron 52, 845–855. [PubMed: 17145505]

Highlights

- A short-term memory trace is encoded in and retrieved from MBOn-γ2α′1

- A single dopamine neuron participates in forming and disrupting this memory trace

- New learning simultaneously disrupts old memory traces while forming new ones
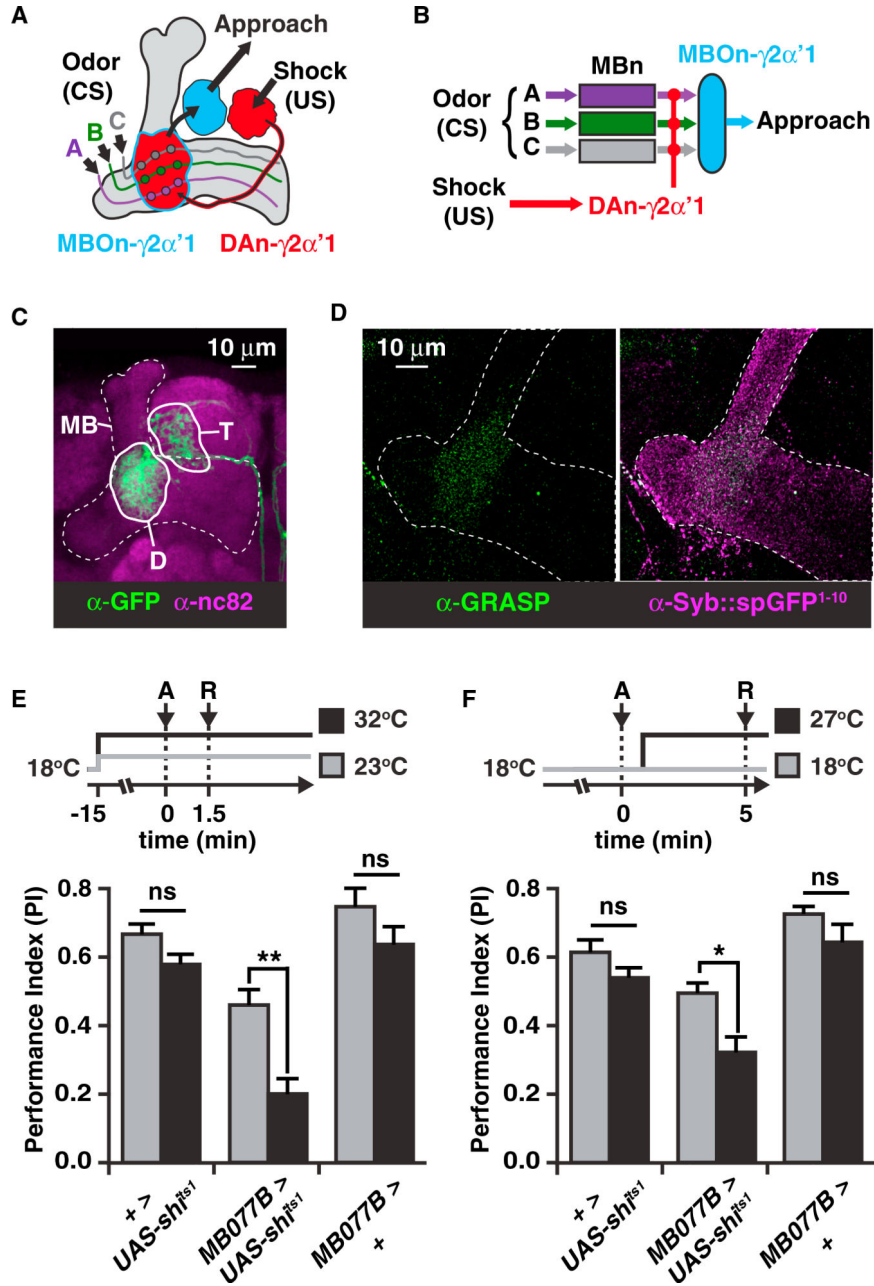
Figure 1. MBOn-γ2α'1 Receives Synaptic Input from MBns, and Its Output Is Required for Aversive Memory Retrieval

(A) Schematic diagram of the γ2α'1 compartment (also referred to as the junction) of the MB (gray shading) showing relevant neurons and pathways. The red objects represent DAn innervation, conveying information about electric shock to this neuropil compartment. The DAn axon terminals overlap the region of innervation by the dendrites of the MBOn-γ2α'1 neuron (red region outlined in blue). Circles represent MBn to MBOn synapses. Odors A, B, and C activate axon fibers from individual MBns (colored lines).

(B) Simplified circuit diagram of (A), with odor inputbeing conveyed by MBns, and approach behavior biased by the output of MBOn-γ2α'1.

(C) MBOn-γ2α′1 morphology visualized using *MB077B-gal4 > myr:GFP* (see inset of Figure S1A). D, dendrites; T, presynaptic terminals.

(D) Reconstituted GFP across the MBn to MBOn-γ2α′1 synapses visualized using GRASP immunostaining (left) overlaid on the collection of MBn presynaptic terminals detected by syb::spGFP[1–10] immunostaining (right).

(E and F) MBOn-γ2α′1 output was blocked either during both acquisition, A, and retrieval, R, of short-term aversive memory (E), or specifically during the retrieval of short-term aversive memory (F).

Time in protocols is with respect to the beginning of odor-shock association. Bar plots represent the mean with error bars equal to + SEM in this figure and others. Two-way ANOVA followed by Bonferroni post hoc tests. $*p < 0.01$, $**p < 0.0001$; n = 7–8. ns, not significant; UAS, upstream activation sequence.

See also Figure S1.
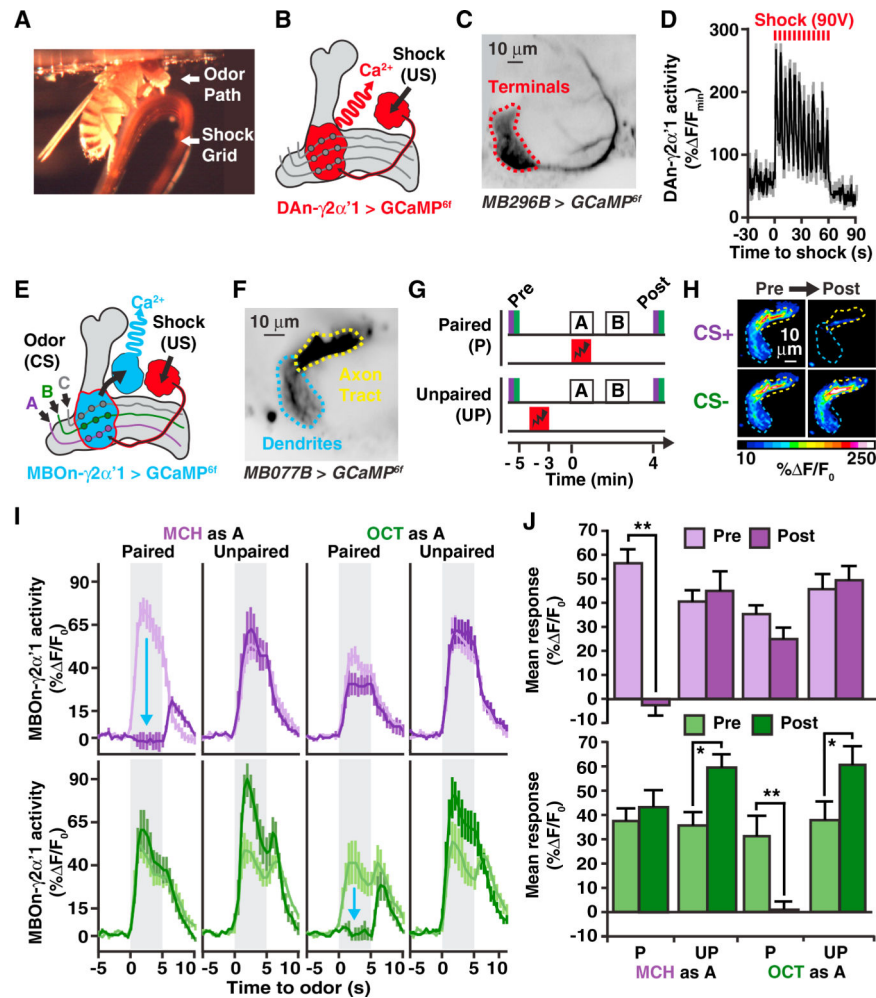
Figure 2. Aversive Classical Conditioning Creates Robust Short-Term Plasticity in MBOn-γ2α′1

(A) Photograph of the *in vivo* functional imaging setup showing a fly standing on an electric shock grid prepared to receive odor and/or electric shock stimuli. The top of the head capsule is obscured but positioned just below the microscope objective.

(B) Schematic of circuits and tools used to collect data in (C) and (D).

(C) GCaMP[6f] specifically expressed in DAn-γ2α′1 axon terminals using *MB296B-gal4* (red-dotted outline). Mean time series projection of GCaMP[6f] fluorescence from a 30-s time window before electric shock.

(D) Time course of GCaMP[6f] responses in DAn-γ2α′1 terminals with electric shock exposure (90V, 12×) used in (G) showing the mean and SEM of n = 8 animals.

(E) Schematic of circuits and tools used to collectdata shown in (F)–(J). Odors (CS) activate sparse MBns that stimulate MBOn-γ2α′1 (blue) via synaptic connections (circles). Electric shock (US) activates DAn-γ2α′1 (red) with DA release modulating MBn:MBOn-γ2α′1 functional connectivity.

(F) Mean time series projection of baseline GCaMP[6f] driven by *MB077B-gal4* in the MBOn-γ2α′1 dendrites and its axon tracts (tdTomato was also expressed but not used in the analysis). The area labeled "Axon Tract" resides outside the MB neuropil and probably contains axon terminals in addition to the axon tracts, explaining its breadth.

(G) Paired and unpaired conditioning protocols used to collect data shown in panels (H)–(J). Odor A and B are defined as the first and second odors given during the training, respectively. GCaMP[6f] responses were monitored before conditioning (pre) to establish basal responses to odor stimulation. The CS$^+$ was presented paired or unpaired with electric shock pulses. A CS$^-$ odor was presented as a control. Changes in response properties were measured during odor stimulation after conditioning (post). Timeline (bottom) indicates time points relative to the start of CS/US association, including the start of pre and post responses and the end of shock in the unpaired protocol.

(H) Pseudocolored peak responses of MBOn-γ2α′1 axons and dendrites to the CS$^+$ (MCH) and CS$^-$(OCT) before and after a paired protocol.

(I) Time course of the dendritic Ca^{2+} responses of MBOn-γ2α′1 during a 5-s exposure (gray-shaded regions) to either MCH (top) or OCT (bottom) before (light-colored line) and after (dark-colored line) paired or unpaired protocols. Traces show the average response (±SEM) across all flies tested. The blue arrows indicate the depressed response due to paired conditioning.

(J) Mean dendritic response during odor exposure before (pre) and after (post) conditioning protocols from data shown in (I).

Two-way repeated-measures ANOVA with Bonferroni post hoc tests. *$p < 0.05$, **$p < 0.001$; n = 8–10.

See also Figure S2.
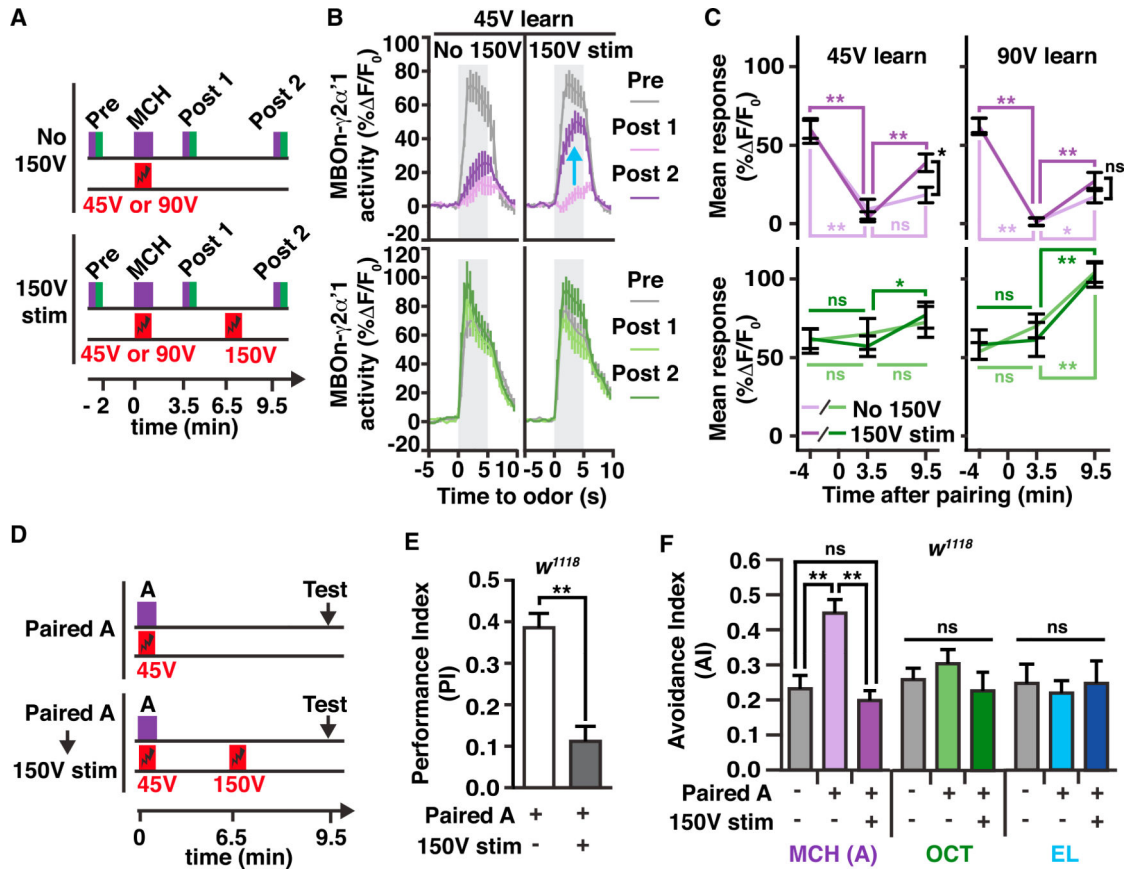
Figure 3. US Pathway Stimulation Restores MBOn-γ2α′1 Responses Previously Depressed by Learning and Causes Behavioral Forgetting

(A) Conditioning protocols used to collect data shown in (B) and (C) and Figures S3A–S3D. GCaMP[6f] responses in MBOn-γ2α′1 (*MB077B-gal4 > GCaMP[6f]*) to odor (pre, post 1, and post 2) were monitored before odor/shock pairing, after the pairing (45 V, 12× or 90 V, 12×), and after either strong 150 V, 12× electric shock (150 V stim) or no strong shock (no 150 V), respectively. Timeline (bottom) indicates time points relative to the start of CS/US association, including the start of pre, post 1, and post 2 responses, and the start of 150 V shock.

(B) Time course of dendritic Ca^{2+} responses in MBOn-γ2α′1 for 45 V pairing experiments upon odor exposure (gray-shaded regions) to MCH or OCT before (pre, gray lines), after odor/45 V shock pairing (post 1, light-colored lines), and after either 150 V shock or no shock (post 2, dark-colored lines). The blue arrow indicates the recovered response due to the 150 V stimulation.

(C) Mean dendritic response during the three odor exposures relative to time of learning for data from (A) (light-colored lines, no 150 V; dark-colored lines, 150 V stim). Two-way repeated-measures ANOVA with Bonferroni post hoc tests (comparing across 150 V stim or no 150 V conditions, black asterisk, $*p < 0.05$; or comparing across time points, colored asterisk matched to condition, $*p < 0.05$, $**p < 0.001$; ns, not significant; n = 10–11).

(D) Behavioral conditioning protocols used to collect data in (E) and (F). Twelve electric shock pulses (45 V) were paired with an odor A (e.g., MCH) and then flies were tested for

memory performance(E) or odor avoidance (F) after no intervening stimulus(paired A) or after electric shock stimulation(150 V,12×)(paired A→150 V stim).Timeline (bottom) indicates time points relative to the start of CS/US association, including the start of 150 V shock and the start of behavioral testing.

(E) Performance index (PI) measuring preference of w^{1118} flies between the paired odor A (e.g., MCH) and a second odor (e.g., OCT) after the conditioning protocols illustrated in (D). A positive PI indicates aversion of the flies to odor A. One-way ANOVA with Bonferroni post hoc tests. $**p < 0.0001$; n = 8–12.

(F) Avoidance index (AI) of w^{1118} flies measuring the preference between the paired odor A (MCH), or one of two novel odors, OCT and ethyl lactate (EL), and fresh air after the conditioning protocols illustrated in (D).

One-way ANOVA with Bonferroni post hoc tests. $*p = 0.0039$, $**p < 0.0001$; n = 8–12. See also Figure S3.
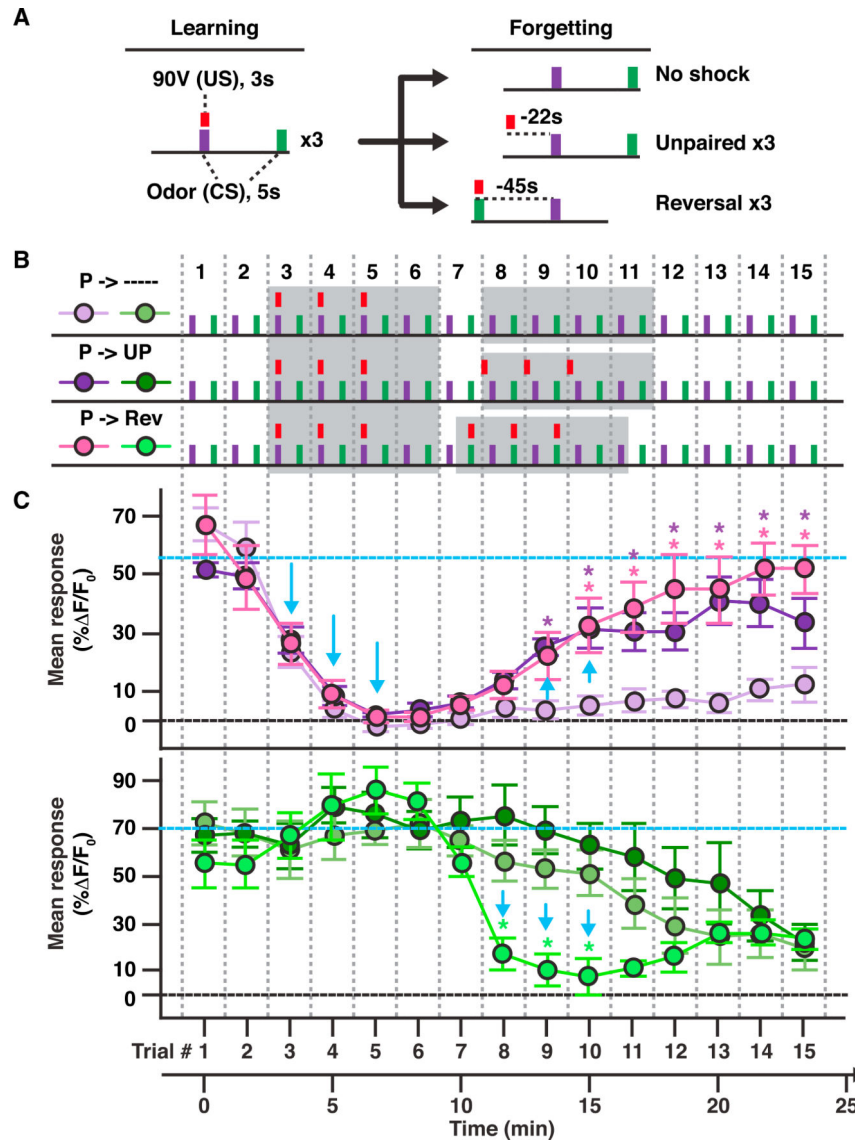
Figure 4. New Learning Simultaneously Depresses MBOn-γ2α′1 Responses toa Paired Odor While Restoring Responses to a Previously Depressed Odor

(A) Simplified diagram of conditioning protocolsused to collect data for (C) and Figure S4, consisting of three short odor-shock pairings (learning) with a 45-s intertrial interval (ITI) between CS+ and CS− followed by several forgetting protocols (forgetting). The red bar represents a single 3-s, 90-V shock.

(B) Conditioning protocols used to collect data in (C). P, paired; UP, unpaired; Rev, reversal. The gray-shaded areas of the protocols highlight the learning trials (trials 3–6) and the forgetting trials (trials 7–11).

(C) The mean dendritic Ca^{2+} responses of MBOn-γ2α′1 (*MB077B-gal4 > GCaMP^{6f}*) during odor trials 1–15 for MCH (top) and OCT (bottom) depicted using the color scheme shown in (B).

Blue arrows indicate depression or recovery of responses. Blue dashed lines show the initial response level. Two-way repeated-measures ANOVA with Bonferroni post hoc tests. *p < 0.05 between both unpaired and Rev groups relative to the control decay; n = 8. See also Figure S4.
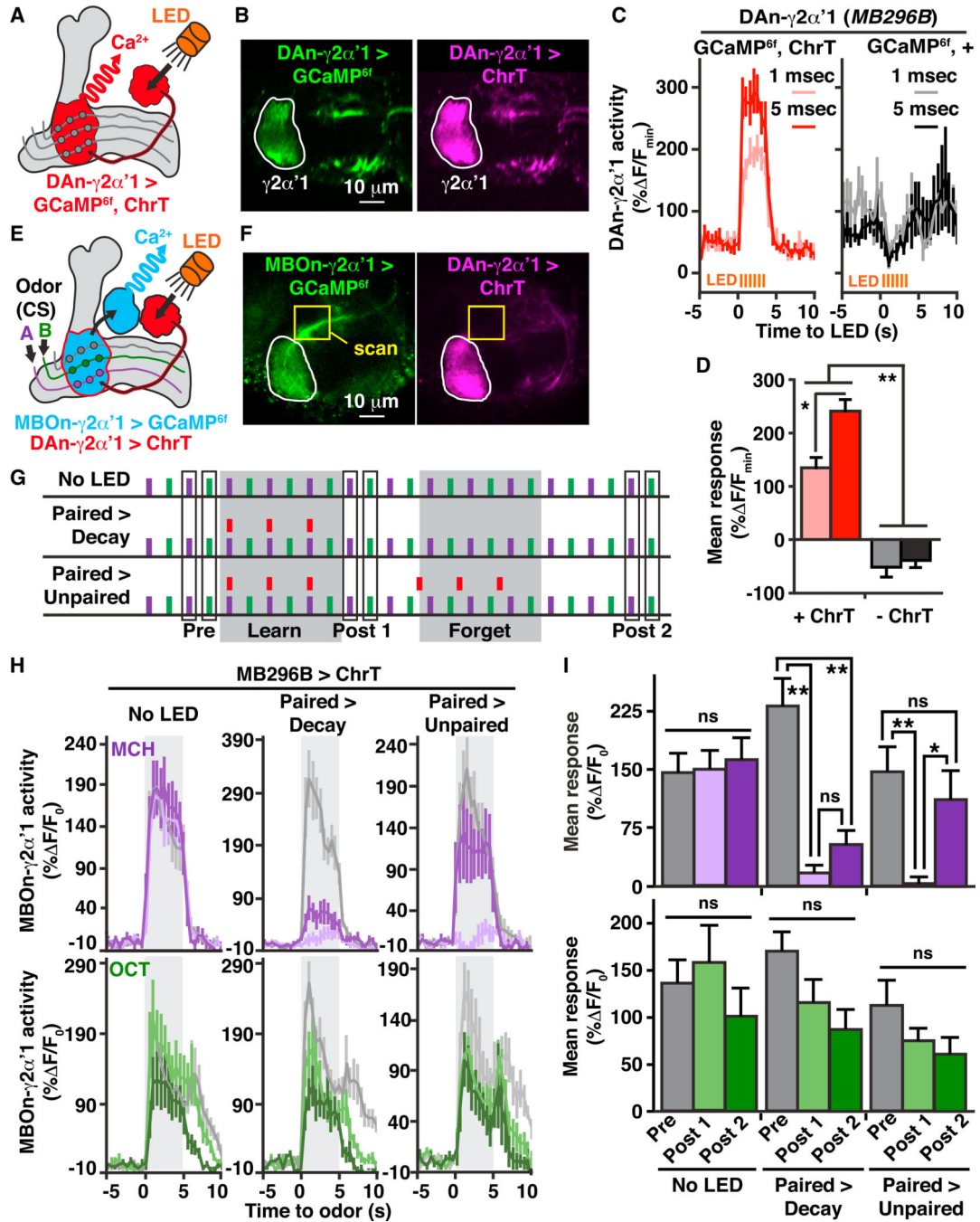
Figure 5. Optogenetic Activation of DAn-γ2α′1 Fully Depresses or Restores MBOn-γ2α′1 Odor Responses When Paired or Unpaired with Odors, Respectively

(A) Schematic illustration of circuits and tools used to collect data in (B)–(D).

(B) GCaMP[6f] (left) and Chrimson::tdTomato (ChrT, right) expression in DAn-γ2α′1 with the region of interest outlined and analyzed in (C) and (D).

(C) Time course of the mean (±SEM) for axonal GCaMP[6f] responses in DAn-γ2α′1 during a 3-s train (2 Hz) of 1 or 5 ms LED pulses presented to flies with (ChrT) or without ChrT expression (n = 8).

(D) Mean response of DAn-γ2α′1 during LED light exposure from data shown in (C). Two-way repeated-measures ANOVA with Bonferroni post hoc tests. *p < 0.01, **p < 0.0001; n = 8.

(E) Schematic of circuits and tools and stimuli used to collect data shown in (F)–(I).

(F) Example images of GCaMP^{6f} (left) expression in MBOn-γ2α′1 using R25D02-lexA and Chrimson:tdTomato (right, ChrT) expression in DAn-γ2α′1 using *MB296B-gal4*. The yellow box indicates the two-photon scanning region of the MBOn-γ2α′1 axon to prevent unwanted activation of ChrT expressed in the DAn-γ2α′1 terminals (area outlined in white).

(G) Stimulus protocols used for experiments shown in (H) and (I). MCH (5 s) and OCT (5 s) odor stimuli were presented with a 45-s ITI. The red bars represent 3-slight stimuli (LED). The MBOn-γ2α′1 axon was scanned before (pre) and after (post 1) a learning period (learn) during which odor and light stimuli were paired or light was not presented (no LED), and after (post 2) a forgetting period (forget) during which either three light pulses were presented unpaired with MCH (22 s prior) (paired > unpaired) or light was not presented (no LED and paired > decay). Timing of odor trials is the same as the timeline in Figure 4C.

(H) Time course of axonal GCaMP^{6f} responses during a 5-s odor exposure (gray-shaded region) to MCH or OCT at the pre (gray lines), post 1 (light-colored lines), and post 2 (dark-colored lines) time points shown in (G) for flies expressing ChrT in DAn-γ2α′1 and GCaMP^{6f} in MBOn-γ2α′1.

(I) Mean response during odor exposure of MBOn-γ2α′1 colored to match the data in (H). Two-way repeated-measures ANOVA with Bonferroni post hoc tests. *p < 0.01, **p < 0.001; n = 8–9; ns, not significant.

Learning
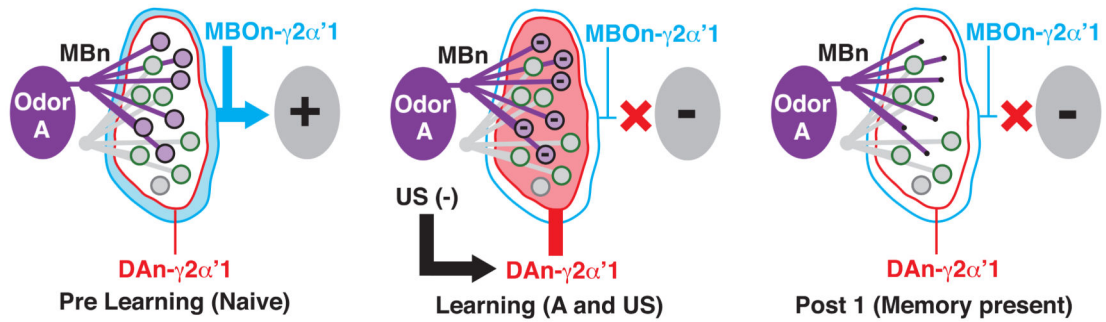
Forgetting / New Learning
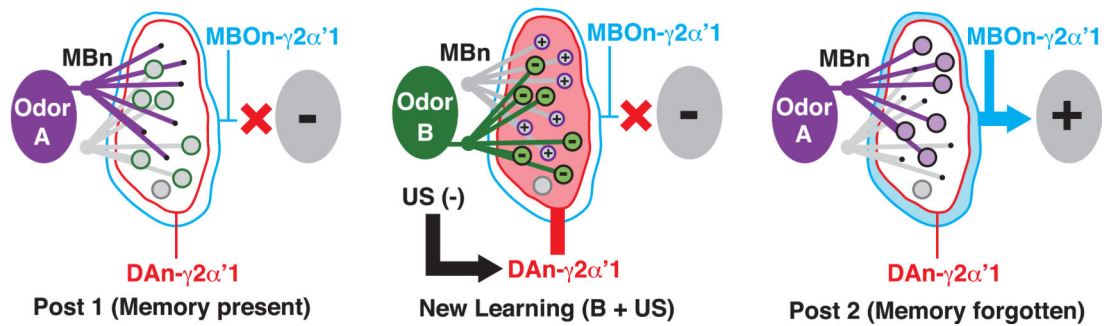
Figure 6. Model for DAn-Mediated Memory Updating in the γ2α′1Compartment

Learning: associative learning specifically depresses MBn/odor synaptic input to MBOn-γ2α′1, thus inhibiting CS$^+$-odor-driven approach behavior. In the naive or prelearning state, MBn:MBOn connectivity is strong and similar between novel odors (magenta and green), indicated by the large circles, to bias odor-driven approach. However, when odor A (magenta) activation of MBn:MBOn synapses is paired with aversive stimulus induced DAn-γ2α′1 activation (US[-], red), (learning [A and US]), the co-activated synapses become depressed (- sign within circle), blocking approach behavior driven by odor A in this compartment (post 1 [memory present]).

Forgetting/New Learning: when synaptic memory is present, aversive stimuli by themselves or when associated with a new odor can drive forgetting by restoring the depressed synapses. After initial learning to odor A (post 1 [memory present]), if DAn-γ2α′1 activation occurs in conjunction with a new odor (B, green), new learning occurs (new learning [B + US]), with DAn triggering depression of odor B synapses (- sign within circle) and the restoration of previously depressed synapses (+ sign within circle), thus disrupting the memory trace and causing forgetting (post 2). Hence, during one learning event (new learning), two relatively independent sets of synapses (those not overlapping between odors A and B) are either depressed or restored, so that learning and forgetting can occur in parallel. Note that this model represents events occurring with weak memory traces. Strong memory traces may also be removed via similar mechanisms over longer periods of time or by stronger "forgetting" stimuli.

REAGENT or RESOURCE	SOURCE	IDENTIFIER
Antibodies		
Rabbit polyclonal anti-GFP	ThermoFischer	Cat#A11122; RRID: AB_221569
Mouse monoclonal anti-nc82	University of Iowa Developmental Studies Hybridoma Bank	RRID: AB_2314866
Mouse monoclonal anti-GFP	Sigma-Aldrich	Cat#G6539; RRID: AB_259941
Alexa 488 goat polyclonal anti-rabbit IgG	ThermoFisher	Cat#A11008; RRID: AB_143165
Alexa 633 goat polyclonal anti-mouse IgG	ThermoFisher	Cat#A21052; RRID: AB_2535719
Alexa 488 goat polyclonal anti-mouse IgG	ThermoFisher	Cat#A11029; RRID: AB_138404
Alexa 633 goat polyclonal anti-rabbit IgG	ThermoFisher	Cat#A21070; RRID: AB_2535731
Experimental Models: Organisms/Strains		
D. melanogaster: *w*[1118]: w[1118];+;+	Bloomington Drosophila Stock Center	Cat#3605
D. melanogaster: R25D01-lexA: w[1118]; P{GMR25D01-lexA}attp40;+	Jenett et al., 2012 / Bloomington Drosophila Stock Center	Cat#53519
D. melanogaster: R13F02-gal4: w[1118]; +; P{GMR13F02-gal4}attp2	Jenett et al., 2012 / Bloomington Drosophila Stock Center	Cat#48571
D. melanogaster: MB077B-gal4: w[1118]; P{R25D01-p65.AD}attP40; P{R19F09-GAL4.DBD}attp2	Aso et al., 2014a /Bloomington Drosophila Stock Center	Cat#68283
D. melanogaster: MB296B-gal4: w[1118]; P(R15B01-p65.AD)attp40; P{R26F01-GAL4.DBD}attp2	Aso et al., 2014a /Bloomington Drosophila Stock Center	Cat#68308
D. melanogaster: UAS-shi[ts1]: w[1118];;P{JFRC100–20XUAS-TTS-shibire(ts1)-p10}VK0005	Pfeiffer et al., 2012	N/A
D. melanogaster: UAS-GCaMP[6f]: w[1118]; P{20XUAS-IVS-GCaMP6f}attp40; +	Chen et al., 2013 / Bloomington Drosophila Stock Center	Cat#42747
D. melanogaster: UAS-myr::GFP: w[1118]; +; P{10XUAS-IVS-myr::GFP}attp2	Pfeiffer et al., 2010 / Bloomington Drosophila Stock Center	Cat#32197
D. melanogaster: UAS-myr::tdTomato: w[1118]; +; P{10XUAS-IVS-myr::tdTomato}attp2	Pfeiffer et al., 2010 /Bloomington Drosophila Stock Center	Cat#32221
D. melanogaster: lexAop-CD4::spGFP11: w[1118]; P{lexAop-CD4::spGFP11}; +	Macpherson et al., 2015 /	N/A
D. melanogaster: UAS-syb::spGFP1–10: w[1118]; +; P{UAS-syb::spGFP1–10}	Macpherson et al., 2015	N/A
D. melanogaster: lexAop-GCaMP[6f]: w[1118]; P{13XLexAop2-IVS-GCaMP6f-p10}su(Hw)attp5; +	Bloomington Drosophila Stock Center	Cat#44277
D. melanogaster: UAS-Chrimson::tdTomato (Chr): w[1118]; +; P{20XUAS-IVS- Syn21-Chrimson::tdTomato-3.1}VK0005	Hoopfer et al., 2015	N/A